Development of Thin-Film Nanocomposite Membranes with Metal-Organic Frameworks for PFAS Removal from Drinking Water

DEPARTMENT OF PROCESS AND LIFE SCIENCE ENGINEERING | LUND UNIVERSITY

NABILA AULIA LAELY PUTRI | MASTER THESIS 2026

Development of Thin-Film Nanocomposite Membranes with Metal-Organic Frameworks for PFAS Removal from Drinking Water

by

Nabila Aulia Laely Putri

Division of Chemical Engineering
Department of Process and Life Science Engineering
Lund University

May 2026

Supervisor: **Mariona Battestini Vives & Beatriz Zornoza**
Co-supervisor: **Dalia Refaat**
Examiner: **Frank Lipnizki**

Postal address
Box 124
SE-221 00 Lund, Sweden
Web address
http://www.ple.lth.se

Visiting address
Kemicentrum
Naturvetarvägen 22
223 62 Lund, Sweden

Telephone
+46 46-222 82 85
+46 46-222 00 00

Preface

First and foremost, I would like to express my deepest gratitude to Allah SWT for His blessings, mercy, and guidance, which have enabled me to complete this research and master's thesis.

This thesis would not have been possible without the support, encouragement, and kindness of many people. I would therefore like to take this opportunity to express my sincere appreciation to those who have contributed to this journey.

I am deeply grateful to my beloved parents, Bapak Edy Purnomo, S.Pt., and Ibu Widijaningrum, S.E., for their endless love, prayers, patience, and unwavering support. I am also sincerely thankful to my siblings, Fadhila and Callysta, for their love, encouragement, and constant presence throughout this journey. My family's belief in me has been one of my greatest sources of strength throughout my studies.

I would like to express my sincere gratitude to Dr. Mariona Battestini-Vives for her supervision, guidance, and support during the experimental work at Lund University. I am also very grateful to Dr. Beatriz Zornoza and Dr. Dalia Refaat for their guidance, scientific input, and support during the membrane development and characterization work at the University of Zaragoza. Their knowledge, patience, and encouragement have greatly helped me throughout this thesis process.

I would also like to thank Dr. Frank Lipnizki for serving as the examiner of this thesis and for his valuable time, advice, and constructive feedback.

My appreciation also goes to Andoni, Laura, Jose, and Marta for their help, kindness, and support during my research work in Zaragoza. Their assistance in the laboratory and their willingness to share knowledge made the research process smoother and more meaningful.

I gratefully acknowledge the European Commission – Education, Audiovisual and Culture Executive Agency (EACEA) for the Erasmus Mundus scholarship under the MESD programme, Project number 101081874, Call ERASMUS-EDU-2022-PEX-EMJM-MOB. I would also like to thank the Servicio General de Apoyo a la Investigación-SAI and ELECMI ICTS Laboratorio de Microscopías Avanzadas (LMA) at Universidad de Zaragoza for their technical support.

I am especially thankful to my dear friends, Kate, Nika, Bat, Sarah, Inna, and Icha, for their constant encouragement, prayers, motivation, and friendship. Their presence has brought warmth and strength throughout this journey.

Finally, I would like to thank everyone who has contributed, directly or indirectly, to the completion of this thesis. Although I may not be able to mention each person individually, every form of help and support has been deeply appreciated.

Generative AI tools were used in the preparation of this thesis. ChatGPT by OpenAI was used for language correction, grammar polishing, improving readability, and preparing rough drafts of schematic figures. Canva AI was used to finalize some schematic figures. All AI-assisted content was reviewed, edited, and verified by the author, who takes full responsibility for the final content, interpretation, and scientific accuracy of this thesis.

Popular Scientific Summary

PFAS, or per- and polyfluoroalkyl substances, are man-made chemicals which have come to be referred to as "forever chemicals" due to the fact that these substances are very hard to degrade in the environment. These chemicals have become ubiquitous in many different types of manufactured items including firefighting foam, non-stick cookware, waterproof clothing, and food wrapping. Due to the nature of PFAS, when released into the environment PFAS can migrate through soil and groundwater until potentially reaching a source of drinking water. Therefore, the need exists for viable remediation options to remove PFAS from water so as to prevent further degradation to human health and the environment.

One area of research being explored for removing contaminants from water is through membrane filtration. Membrane filtration uses a semi-permeable membrane as a filter where pressure pushes water through the membrane allowing water molecules to pass through while preventing larger contaminants from passing through. Specifically, nanofiltration membranes are an attractive option because they allow smaller solutes to pass through while requiring significantly less force than reverse osmosis. One challenge however remains with nanofiltration membranes, specifically maintaining both high water flow rates and good contaminant removal.

The objective of this thesis was to investigate if by incorporating Metal Organic Frameworks (MOFs), into the selective layer of a nanofiltration membrane would provide enhanced membrane performance. MOFs are highly ordered porous crystalline materials whose structure and chemistry can be controlled. As such, MOFs are an ideal additive material for developing new membranes with increased water flux and improved surface characteristics.

Several MOFs were synthesized and dispersed within polyamide-based thin film nanocomposites. Following synthesis and dispersion, all membranes were characterized based on their structural properties, surface characteristics, and water filtration behaviors. The data obtained indicated that the type of MOF used and its concentration greatly influenced the formation of the membrane and how freely water could pass through each respective membrane. Results indicate that some membranes developed using MOFs exhibited negligible or zero measurable water flux indicating that incorporation of MOFs does not inherently enhance membrane performance.

Of those membranes studied, the membrane containing 0.1 wt.% ZIF-8 demonstrated the most well-balanced performance regarding enhanced water permeability, reduced fouling propensity, excellent hydraulic recoveries upon cleaning, and higher-than-unmodified polyamide membrane filtration fluxes. A second MOF examined in this study, UiO-66-NH2, did demonstrate improvements in water transport; however, observable defects and particle aggregation in this particular system complicated interpretation of its performance relative to other systems.

In general terms, this thesis demonstrates that MOF-modified nanofiltration membranes possess significant promise for future applications involving PFAS contaminated water treatment; however, critical considerations should be given to selecting an appropriate MOF species, optimal loadings levels, and effective dispersal methods.

Summary

This thesis investigates the development of metal–organic framework (MOF)-modified thin-film nanocomposite membranes for potential PFAS removal from drinking water. The work focuses on how MOF type and loading influence membrane morphology, surface properties, and hydraulic performance when incorporated into a polyamide selective layer.

Five MOFs, namely ZIF-8, ZIF-L, ZIF-94, NH_2-ZIF-8, and UiO-66-NH_2, were synthesized and evaluated as nanofillers in polyamide thin-film nanocomposite membranes prepared by interfacial polymerization on commercial polysulfone supports. The synthesized MOFs and prepared membranes were characterized using scanning electron microscopy (SEM), energy-dispersive X-ray spectroscopy (EDX), Fourier transform infrared spectroscopy (FTIR), X-ray diffraction (XRD), thermogravimetric analysis (TGA), and water contact angle measurements. Preliminary pure water flux screening was used to identify hydraulically workable membrane formulations before further crossflow filtration testing.

The characterization results confirmed the successful synthesis of the selected MOFs and showed that MOF incorporation affected membrane morphology and wettability. ZIF-8-modified membranes displayed a relatively homogeneous morphology, whereas UiO-66-NH_2-modified membranes showed visible aggregation and defects. EDX analysis supported MOF incorporation through the detection of Zn in ZIF-based membranes and Zr in UiO-66-NH_2-modified membranes. Water contact angle measurements showed opposite wettability trends for the two main MOFs: ZIF-8 tended to increase the contact angle at higher loading, while UiO-66-NH_2 increased membrane hydrophilicity.

Filtration results showed that membrane performance depended strongly on MOF identity, loading, and selective-layer integrity. ZIF-L and NH_2-ZIF-8 resulted in no measurable flux during preliminary screening, while ZIF-94 showed very low flux. ZIF-8 and UiO-66-NH_2 were therefore selected for further evaluation. UiO-66-NH_2 at 0.1% (w/v) showed the highest initial water permeability among the PA-coated membranes, but this result should be interpreted with caution due to visible defects and aggregation. In contrast, ZIF-8 at 0.1% (w/v) showed the most balanced hydraulic performance, combining relatively high water permeability, low fouling factor, good hydraulic recovery, high PFAS filtration flux, and more homogeneous morphology.

Overall, this work demonstrates that MOF incorporation can improve the hydraulic performance of polyamide nanofiltration membranes when the MOF type and loading are properly selected. ZIF-8 at 0.1% (w/v) was identified as the most promising formulation in this study.

Table Of Contents

1. Introduction

1.1 Background

For many years, per- and polyfluoroalkyl substances (PFAS), a large family of synthetic fluorinated chemicals, have been widely used in industrial applications and in commercial products (e.g. fire-fighting foams, surface coatings, fabrics, food packaging, and non-stick and waterproof materials) due to their outstanding thermal and chemical resistance. The excellent chemical stability provided by the strong carbon-fluorine bonds is responsible for this property (Buck et al., 2011). Although this chemical stability is the reason why PFAS have been so widely adopted in industry and commerce, it is also one of the reasons why they persist as harmful environmental pollutants.

The primary route of entry of PFAS into public drinking water supplies is through transportation via the soil, groundwater and/or surface water. Once in contact with a municipal water supply systems, these substances can travel downstream until they reach a drinking water source. The importance of this pathway lies in the fact that municipal drinking water supplies may become a significant contributor to total lifetime human exposure to both short- and long-chain PFAS. In Uppsala, Sweden, historical usage of aqueous film-forming foams resulted in drinking water contamination. Following remedial actions, long-term biomonitoring indicated that drinking water remained an exposure pathway for first-time mothers (Gyllenhammar et al., 2025). Similar exposures have occurred in Ronneby, Sweden, where extremely high levels of PFAS were measured in municipal drinking water. The elevated levels of PFAS measured in Ronneby were due to historical use of firefighting foams at an adjacent airport. A registry-based cohort study conducted by Hammarstrand et al. (2021) demonstrated that women who experienced the greatest estimated drinking water exposure were associated with a higher incidence of polycystic ovarian syndrome and potentially uterine leiomyomas. While there are many uncertainties regarding health impacts associated with PFAS exposure, these examples demonstrate that municipal drinking water can serve as an additional exposure pathway for populations exposed to contaminated water sources.

Increasing awareness of the presence, persistence and potential impact on human health of PFAS has enhanced the demand for effective treatment methodologies to remove PFAS from public drinking water systems. It appears that treatment technologies will be critical for removing PFAS from potable water supplies prior to prolonged exposure. Treatment is necessary due to the highly stable nature of PFAS, combined with their high solubility in water and typically low concentration in complex water matrices.

1.2 Membrane filtration for drinking water treatment

Membrane filtration is a membrane-based separation technology in which a semi-permeable membrane acts as a selective barrier for two phases. In the context of drinking water treatment, the membrane will allow clean water to pass through and retain both soluble and insoluble contaminants based upon the pore-size of the membrane, its internal morphology, surface chemical properties, and operational parameters. Pressure differences across the membrane that drive membrane filtration are called transmembrane pressures (TMP). With respect to their separation ranges, pressure driven membrane processes can be classified into Microfiltration (MF), Ultrafiltration (UF), Nanofiltration (NF), and Reverse Osmosis (RO) (Mulder, 1996; Baker, 2012).

Each membrane process is applicable for the treatment of different types of contaminants. For example, MF and UF are primarily applied for the removal of suspended particles, colloidal particles, bacteria and large molecular weight compounds; whereas NF and RO are typically used to separate small, dissolved compounds. RO has the most restrictive pores of all pressure driven membrane processes and therefore can remove salt from water as well as other low molecular weight compounds at relatively high pressures. NF membranes have less restrictive pores than those of RO membranes and are often used for water softening, removal of natural organic matter (NOM) and separation of multivalent ion/molecule pairs as well as organic micropollutants. Due to their intermediate selectivity characteristics, NF membranes often provide a good compromise between contaminant rejection capabilities and required operation pressure (Baker, 2012; Petersen, 1993).

Since membrane filtration can act as a physically-based separation mechanism that can be easily incorporated with existing drinking water treatment systems, membrane filtration is becoming increasingly popular among treatment technologies. Nevertheless, membrane performance is influenced by a number of additional factors beyond just the pore size of the membrane. Membrane charge, hydrophilic/hydrophobic properties, fouling potential, feedwater composition, and hydrodynamics surrounding the membrane are some examples of these influences. For dissolved organic compounds like PFAS, the influence of size-exclusion effects, electrostatic attraction/repulsion effects, and solute – membrane interaction/solubility effects make membrane material selection/design critical in maximizing PFAS removal rates, particularly for NF membranes (Casella et al., 2026).

1.3 PFAS removal from drinking water

Conventional drinking water treatment methods are typically insufficient for PFAS removal. Conventional processes such as coagulation, sedimentation, and sand filtration were not designed to remove dissolved organic compounds such as stable PFAS. Full-scale drinking water treatment process studies have also demonstrated that PFAS removal is significantly dependent on compound structure, with longer chain PFAS being removed more effectively than shorter chain compounds (Kim et al., 2020). This creates a problem because shorter chain PFAS are often more mobile within water and may be difficult to retain using traditional methods.

Therefore, advanced treatment techniques such as adsorption, ion exchange, reverse osmosis (RO) and nanofiltration (NF) have been increasingly investigated. While activated carbon and ion exchange resin technology can remove PFAS, they frequently demonstrate reduced efficiency for removing shorter chain compounds and generate contaminated spent media that require additional handling. Membrane processes offer attractive alternatives because they can create a physical barrier against dissolved contaminants. Recent reviews show that RO generally achieves high rejection rates of PFAS, while NF offers a lower-pressure alternative with promising performance especially for longer-chain PFAS (Casella et al., 2026; Liu et al., 2025).

However, even though NF has shown great promise as a technique for removing PFAS from drinking water, its performance remains strongly dependent upon membrane chemistry, pore size/structure, charge density, and composition of the surrounding water matrix. Additionally, higher rejection rates of shorter chain PFAS are typically obtained at the expense of lower permeability of water through the membrane. Therefore, developing new NFmembranes should focus not only on improving PFAS rejection but also on maintaining sufficient water flux and operational stability.

1.4 Thin Film Composite Nanocomposite Membranes for PFAS removal

Conventional high-performance NF membranes are primarily based on thin film composite membranes composed of a mechanically strong porous support and a thinner selectively permeable layer of polyamide. The appeal of such membrane configurations lies in the fact that the support provides structural integrity to the membrane, while the selectively permeable layer determines both water transport characteristics and solute rejection. The selective layer is typically formed via an interfacial polymerization process, allowing for the creation of very thin layers of polyamide film on the surface of the membrane.

Although they provide several advantages over prior technologies, conventional polyamide-based thin film composite membranes continue to be subject to a trade-off related to selectivity and permeability. Increasing the density of the selectively permeable layer may increase rejection of PFAS; however, increased layer thickness may decrease water flux. On the other hand, increasing the permeability of the membrane may result in less than optimal rejection levels, particularly for smaller and more mobile PFAS. As a consequence, researchers are now actively developing new membrane architectures to modify the selectively permeable layer using functional nanomaterials.

One method to achieve improved separation characteristics for PFAS removal involves the incorporation of functional nanomaterials into or adjacent to the polyamide selectively permeable layer. Through this approach, membrane surface chemistry, morphology, hydrophilicity, and transport pathways may all be modified. Since rejection of PFAS is dependent not only upon size exclusion, but also upon electrostatic interactions, hydrophobic/hydrofluoro interactions between PFAS molecules and the membrane material, membrane charge, and effects associated with the water matrix (Casella et al., 2026), modification of these factors may lead to significant improvements in membrane performance.

Several nanofiller types have been considered for inclusion into thin film nanocomposites (TFN); among them, metal – organic frameworks (MOFs) present some unique features due to their ability to tailor the pore structure and surface chemistry through the selection of metal ions used as nodes and organic linkers used to form ligands. More recently, there has been a growing interest in understanding the nature of PFAS-MOF interactions. Interactions include electrostatic attraction, coordination to metal sites, hydrophobic/fluorophilic interactions, and/or confinement within pores (Mashkoor et al., 2026). Thus, when incorporated into membranes, MOFs could serve as both nanofillers and as components that control transport through the membrane and modify interfacial properties.

The use of MOFs in PFAS-selective NF membranes appears to be significantly less extensive studied than the use of many other nanomaterial systems. Most existing research reports have focused on individual MOF compositions (Liu et al., 2025), thereby limiting evaluation of how framework chemistry, functional groups, and morphology affect membrane performance. A comparative evaluation of multiple MOFs under identical membrane fabrication protocols is therefore necessary to fully appreciate the potential roles of MOFs in thin film nanocomposite membranes.

1.5 Aim of the Study

The main objective of this project is the development of MOF-modified thin film nanocomposite (TFN) membranes and their evaluation for PFAS removal from drinking water. The study

focuses on how different MOF types influence membrane properties and filtration performance when incorporated into a polyamide selective layer.

The selected MOFs are ZIF-8, ZIF-94, ZIF-L, NH_2-ZIF-8, and UiO-66-NH_2. These materials were chosen to represent different framework chemistries, functionalities, and expected interactions with the polyamide layer. By preparing the membranes under comparable fabrication conditions, this work aims to clarify the effect of MOF identity on membrane morphology, surface properties, water permeability, and PFAS removal potential.

To achieve this aim, the work was divided into the following steps:

1. Reviewing the state of the art on PFAS removal by NF and MOF-modified membranes;
2. Synthesizing and characterizing selected MOFs for membrane incorporation;
3. Fabricating polyamide thin-film composite (TFC) and MOF-modified thin-film nanocomposite (TFN) membranes on commercial PSf porous membranes acting as mechanical supports;
4. Characterizing the prepared membranes using SEM, EDX, FTIR, XRD, water contact angle, and TGA;
5. Screening the hydraulic performance of the prepared membranes using pure water flux measurements;
6. Evaluating selected membranes through pure water flux, PFAS filtration, and post-filtration cleaning tests;
7. Discussing the relationship between MOF type, membrane properties, and filtration performance.

This thesis was carried out as a collaborative project between Instituto de Nanociencia y Materiales de Aragón (INMA), University of Zaragoza, Spain, and Lund University, Sweden. MOF synthesis, membrane fabrication, and material characterization were conducted at INMA, at MECANOS group (Membranes and catalysis with nanostructured materials) under the supervision of Dr. Beatriz Zornoza, with laboratory support from Dr. Dalia Refaat. Membrane filtration experiments were mainly conducted at Lund University under the supervision of Dr. Mariona Battestini-Vives.

2 Literature Review

2.1 PFAS Removal using Nanofiltration Membrane Processes

Among membrane processes used to remove PFAS, RO and NF are currently considered among the best methods. NF typically uses less pressure than RO but achieves similar results when it comes to long-chain PFAS compounds (Casella et al., 2026; Liu et al., 2025). However, the removal of dissolved ions by membrane processes may also affect the mineral composition of the treated water. RO can produce water with very low hardness and total dissolved solids, thereby requiring post-treatment or remineralization in drinking-water applications. Although NF generally has a lower overall salt rejection than RO, remineralization may also be required depending on the membrane characteristics, feed-water composition, and extent of mineral removal (Pervov & Spitsov, 2023).

However, NF membrane rejection rates vary depending on PFAS structure. Long-chain PFAS, such as perfluorooctane sulfonate (PFOS) and perfluorooctanoic acid (PFOA), are usually rejected at high levels, whereas short-chain PFAS, such as perfluorobutanoic acid (PFBA) and perfluorobutane sulfonate (PFBS), are generally more difficult to reject because of their smaller molecular size and higher mobility through the membrane selective layer (Casella et al., 2026). Previous studies have also shown that membrane surface charge, pore structure, feed ionic strength, and the presence of natural organic matter can significantly affect PFAS rejection and water permeability (Pla et al., 2025).

Despite the promise of NF, the comparatively lower rejection of short-chain PFAS and the conventional trade-off between solute rejection and water permeability remain significant challenges. Consequently, recent NF membrane development has focused on designing selective layers that outperform those used in conventional commercial membranes.

2.2 Developing a High-Performance Selective Layer Based on Interfacial Polymerization

The majority of the high-performance NF membranes studied today consist of a porous support material coated with a thin polyamide selective layer. Most of these selective layers are produced via interfacial polymerization (IP), which involves the rapid chemical reaction of reactive monomers in two separate, immiscible aqueous and organic phases to produce a highly cross-linked and extremely thin film (Petersen, 1993).

Based on a review by Liu et al. (2025), numerous studies on PFAS removal from water utilizing IP-derived NF membranes confirm that the use of IP remains the predominant method of producing NF membranes capable of selectively separating PFAS. Several different combinations of monomers are utilized in the preparation of these NF membranes. For example, piperazine (PIP) or m-phenylenediamine (MPD) is commonly dissolved in the aqueous phase, while trimesoyl chloride (TMC) is dissolved in the organic phase.

The widespread use of IP is attributed to its versatility. Parameters such as monomer concentration, reaction time, temperature, additives, and curing conditions can be adjusted to modify membrane thickness, cross-linking density, surface properties, and mass-transfer resistance. Thus, IP represents a convenient way to develop PFAS-selective membranes with minimal alteration to the support material.

2.3 Development Of Thin-Film Nanocomposite Membranes To Overcome Limitations Of Conventional Polyamide Membranes

To achieve improvements in permeability and/or selectivity in polyamide NF membranes, researchers have developed a new class of membranes referred to as thin film nanocomposite (TFN) membranes. TFN membranes are generally prepared by incorporating nanoscale fillers into one of the monomer solutions used to form the selective layer or by depositing the fillers onto or within the selective layer during membrane fabrication.

Le et al. (2022) demonstrated that incorporating functionalized MXene nanosheets into thin-film nanocomposite membranes enhanced PFOS rejection and water permeability. GO-based membranes have also shown promising PFAS separation performance; Pla et al. (2025) reported PFOA rejection of up to 95% and demonstrated that membrane loading, thickness, and chemical modification could be adjusted to balance rejection and permeability.

Nanofillers may modify membrane morphology, hydrophilicity, water-transport pathways, and surface charge. However, the exact contribution of each effect is still an active research topic, especially for PFAS separation, where steric, electrostatic, and hydrophobic interactions may occur simultaneously. This uncertainty motivates further investigation of different filler types, including porous fillers such as MOFs.

2.4 Metal–Organic Frameworks As Functional Fillers

MOFs offer potential benefits as nanofillers due to their inherent porous nature and ability to be chemically modified post-synthesis. MOFs are formed by the combination of metal centers and organic linkers. As such, MOFs allow for systematic control over their pore diameters, surface functionalities and overall framework architectures (Furukawa et al., 2013).

With respect to application as membrane filters, MOFs possess several advantages relative to nonporous nanofillers. Accessible internal pores within MOFs may provide additional pathways for water transport through the selective layer. Surface functional groups present on MOFs can increase compatibility with the polyamide matrix and potentially influence contaminant interactions through electrostatic forces. Both characteristics are relevant for the removal of PFAS, where both molecular transport resistances and interfacial forces determine rejection rates.

Reviews have identified MOFs as promising materials for PFAS remediation because of their tunable pore structures, surface functionalities, and potential interactions with fluorinated contaminants (Liu et al., 2025). Nevertheless, only a limited number of studies have specifically examined MOF-containing nanofiltration membranes for PFAS removal, and the available studies have generally focused on individual MOF systems, including ZIF-L and other MOF-based membranes (Bi et al., 2024; Zhang et al., 2024)

2.5 Relevant MOFs for This Thesis

The MOFs selected in this study represent different framework structures, chemical functionalities, and physicochemical properties.

ZIF-8 is one of the most extensively studied zeolitic imidazolate frameworks because of its porous structure and relatively high chemical and thermal stability, making it a suitable reference material for comparison with other ZIF-based fillers (Park et al., 2006). The inclusion of NH_2-ZIF-8 allowed the effect of amine functionalization to be examined. The presence of amine groups on the MOF surface may enhance interfacial compatibility between the MOF particles and the polyamide matrix, thereby providing a basis for comparison with unfunctionalized ZIF-8 (Jo et al., 2022; Muramba et al., 2026).

Bi et al. (2024) obtained interesting results about ZIF-L in membranes for selectively removing PFAS. Therefore, we chose ZIF-L because it represents an example of MOFs, which could be very useful in such applications. ZIF-94 was selected as a linker-modified ZIF to investigate how changes in linker chemistry and framework polarity affect membrane properties. In addition, UiO-66-NH_2 was selected as a representative of zirconium-based MOFs, since they are generally well known for their good resistance against hydrolysis and suitability for use in aqueous systems (Cavka et al., 2008).

Together, these five MOFs provide a comparative basis for studying how framework chemistry, functional groups, and morphology influence the performance of MOF-modified NF membranes for PFAS removal.

2.6 Research Gap and Thesis Positioning

Previous studies have demonstrated that NF is an effective technology for PFAS removal and that IP remains a predominant method for producing selective layers for water-treatment membranes. The incorporation of nanofillers also offers a potential strategy for modifying membrane permeability and selectivity.

Although MOFs have been investigated in nanofiltration membranes, PFAS-focused studies have generally evaluated individual MOF systems rather than directly comparing multiple framework types under the same fabrication and testing conditions (Liu et al., 2025; Casella et al., 2026). It remains unclear whether observed changes in membrane performance arise from the general presence of a porous filler or from the specific chemistry and structure of the selected MOF.

This thesis addresses this gap by comparing ZIF-8, NH_2-ZIF-8, ZIF-L, ZIF-94, and UiO-66-NH_2 within the same TFN membrane fabrication platform. By applying a comparable fabrication approach while varying the MOF type, this work aims to clarify how MOF identity affects membrane morphology, surface properties, water permeability, and PFAS filtration performance.

3 Materials and Methods

3.1 Materials

Commercial polysulfone (PSf) GR70PP membranes from Alfa Laval (Denmark), with a molecular weight cut-off (MWCO) of 20,000 Da, were used as supports for TFC and TFN membrane fabrication. The polyamide selective layer was prepared using m-phenylenediamine (MPD, 99%, Sigma-Aldrich, Spain), trimesoyl chloride (TMC, 98%, Sigma-Aldrich, Spain), sodium chloride (NaCl, 99%, Sigma-Aldrich, Spain), and n-hexane (extra pure, Scharlab, Spain).

Five MOFs, namely ZIF-8, ZIF-L, ZIF-94, NH_2-ZIF-8, and UiO-66-NH_2, were synthesized as nanofillers. Zinc nitrate hexahydrate ($Zn(NO_3)_2 \cdot 6H_2O$), 2-methylimidazole (mIm), 2-aminobenzimidazole (2-ambzIm, 97%), and cobalt nitrate hexahydrate ($Co(NO_3)_2 \cdot 6H_2O$, 98%) were purchased from Sigma-Aldrich (Spain). 4-Methyl-5-imidazole-carboxaldehyde (camIm) was supplied by Acros Chemicals (Spain). Zirconium (IV) chloride ($ZrCl_4$, >99.5%, Alfa Aesar), 2-aminoterephthalic acid (NH_2-BDC, 99%, Thermo Scientific), and formic acid (HCOOH, 90%, Fisher Scientific) were purchased from Thermo Fisher Scientific (USA). Methanol was purchased from Análisis Vínicos (Spain), 1-butanol from Scharlab (Spain), and absolute ethanol (99.5%) and deionized water from Productos Gilca S.C. (Spain).

3.2 Synthesis of Metal–Organic Frameworks

The MOF synthesis procedures were adapted from previously reported methods, with modifications in reagent quantity and washing conditions as required for this work. All synthesized

MOFs were dried at 60 °C overnight unless otherwise specified, ground using a mortar, and stored in sealed vials before membrane fabrication.

3.2.1 Synthesis of ZIF-8

ZIF-8 was synthesized following a methanol-based room-temperature route adapted from Martínez-Izquierdo et al. (2022) & Refaat et al. (2024). Initially, zinc nitrate hexahydrate was dissolved in methanol under stirring until complete dissolution. Then, 2-methylimidazole was added, and the mixture was stirred for 30 min at room temperature. The resulting suspension was transferred into Falcon tubes and centrifuged at 9000 rpm for 10 min. The precipitate was washed with methanol, and the washing–centrifugation step was repeated four times. The obtained solid was dried overnight and ground into a fine powder.

3.2.2 Synthesis of ZIF-L

ZIF-L was synthesized following the procedure reported by Bi et al. (2024), with reagent quantities reduced by half. Cobalt nitrate hexahydrate and 2-methylimidazole were dissolved in deionized water and stirred for 4 h at room temperature. The resulting suspension was centrifuged at 9000 rpm for 20 min. The precipitate was washed with deionized water three times, dried overnight, and ground into a homogeneous powder.

3.2.3 Synthesis of ZIF-94

ZIF-94 was synthesized through a solvent-assisted ligand exchange (SALE) method adapted from Martínez-Izquierdo et al. (2022) & Refaat et al. (2024). First, 4-methyl-5-carboxyaldehyde was dissolved in 1-butanol. ZIF-8 powder was then added to the ligand solution, and the suspension was stirred for 24 h at room temperature. The resulting suspension was centrifuged at 9000 rpm for 10 min. The precipitate was washed with 1-butanol three times, dried overnight, and ground into powder.

3.2.4 Synthesis of NH_2-ZIF-8

NH_2-ZIF-8 was synthesized using a modified literature procedure adapted from (Thompson et al., 2013). 2-Methylimidazole and 2-aminobenzimidazole were dissolved in methanol and stirred at 50 °C for 2 h. In a separate solution, zinc nitrate hexahydrate was dissolved in methanol. After the ligand solution cooled down, the two solutions were mixed and stirred for 1.5 h. The suspension was centrifuged at 9000 rpm for 10 min, and the precipitate was washed with methanol three times. The obtained solid was dried overnight, ground using a mortar, and stored in a vial.

3.2.5 Synthesis of UiO-66-NH_2

UiO-66-NH_2 was synthesized using a solvothermal method adapted from Pina-Vidal et al. (2024). Zirconium chloride and 2-aminoterephthalic acid were dissolved in ethanol, followed by the addition of 30 wt% formic acid in water as an acid modulator. The mixture was sonicated for 10 min and then transferred into an autoclave. The reaction was carried out at 110 °C for 12 h. After cooling, the suspension was centrifuged at 9000 rpm for 10 min. The precipitate was washed three to five times with absolute ethanol and then activated in a vacuum oven at 200 °C for 12 h. The activated powder was ground using a mortar and stored in a vial.

3.3 Cleaning of Commercial PSf Support Membranes

The commercial PSf support membranes were cut into circular pieces with an approximate diameter of 9 cm. Prior to interfacial polymerization, the supports were soaked in distilled water for 1 h. The membranes were then conditioned by immersion in 0.1 wt% NaOH solution at 60

°C for 12 h. After conditioning, the membranes were rinsed thoroughly with distilled water until neutral pH was reached. The cleaned supports were stored in Petri dishes before use.

3.4 Fabrication of Polyamide Thin-Film Composite Membranes

Polyamide TFC membranes were prepared by interfacial polymerization on cleaned PSf support membranes. The aqueous phase was prepared by dissolving 2.0 wt% MPD and 0.5 wt% NaCl in deionized water. The solution was stirred until complete dissolution and prepared fresh before use. The organic phase was prepared by dissolving 0.1 wt% TMC in n-hexane. Because TMC is moisture-sensitive, the organic solution was prepared immediately before use and kept tightly closed.

The PSf support membrane was placed on a flat glass plate with the active side facing upward. Although the support diameter was approximately 9 cm, the area exposed to interfacial polymerization was approximately 8 cm in diameter. The MPD aqueous solution was poured onto the membrane surface until the surface was fully covered and saturated. The membrane was kept in contact with the aqueous phase for 2 min to allow MPD penetration into the top pores of the support. After the contact time, the excess solution was drained and carefully removed using a rubber roller. The membrane surface was maintained wet but not flooded.

The TMC solution in n-hexane was then rapidly poured onto the membrane surface. The interfacial polymerization reaction was allowed to proceed for 30 s, during which a thin polyamide selective layer formed at the interface. After the reaction, the organic phase was removed, and the membrane was left for approximately 1 min. The membrane was then cured in an oven at 70 °C for 5 min to enhance polyamide layer formation and stability.

After curing, the membrane was washed with hexane to remove residual organic phase and subsequently rinsed with deionized water. The prepared membrane was stored in water until characterization or filtration testing.

3.5 Fabrication of MOF-Modified Thin-Film Nanocomposite Membranes

MOF-modified thin-film nanocomposite membranes were prepared by incorporating MOF particles into the organic phase during interfacial polymerization. For the first membrane fabrication set, each MOF was dispersed in the TMC/hexane solution at a loading of 0.1% (w/v). The MOF-containing TMC/hexane suspension was prepared before the interfacial polymerization step and used as the organic phase.

The same interfacial polymerization procedure described for the TFC membrane was applied to all TFN membranes, with the only difference being the addition of MOF particles into the organic phase. This approach allowed the effect of MOF type to be compared under equivalent fabrication conditions.

Additional TFN membranes were prepared using different MOF loadings for selected formulations. ZIF-8-modified membranes were prepared with MOF loadings of 0.05, 0.1, and 0.2% (w/v). UiO-66-NH_2-modified membranes were prepared with MOF loadings of 0.05, 0.1, and 0.2% (w/v). The prepared membranes were stored in water until characterization or filtration testing.

3.6 Membrane Characterization

3.6.1 Scanning Electron Microscopy

Scanning electron microscopy (SEM) was used to observe the surface morphology and cross-sectional structure of the membranes. Membrane samples were cut into approximately 1 cm × 1 cm pieces and dried in an oven at 60 °C. For cross-sectional imaging, dried samples were immersed in liquid nitrogen to freeze the membrane and facilitate brittle fracture. The fractured samples were mounted on SEM supports and coated with palladium before analysis. SEM images were obtained using an Inspect F50 scanning electron microscope (FEI, USA) operated at 10 kV that available at the LMA laboratory.

3.6.2 Fourier Transform Infrared Spectroscopy

Fourier transform infrared spectroscopy (FTIR) was used to identify chemical functional groups in the prepared membranes and MOF powders. Membrane samples were cut into approximately 1 cm × 1 cm pieces and dried in an oven at 60 °C before analysis. FTIR spectra were recorded using a Bruker Vertex 70 FTIR spectrometer (Bruker Optics, Germany) equipped with a Golden Gate diamond ATR attachment and a DTGS detector. Spectra were collected over the wavenumber range of 4000–600 cm^{-1} with a resolution of 4 cm^{-1} by averaging 60 scans.

3.6.3 Thermogravimetric Analysis

Thermogravimetric analysis (TGA) was performed to evaluate the thermal stability of the membranes and MOF powders. Samples were cut into approximately 1 cm × 1 cm pieces and dried at 60 °C before analysis. The TGA measurements were performed using a TGA/DSC 1 SF/1100 instrument (Mettler Toledo, Switzerland) equipped with an alumina 70 µL sample holder, available at the MECANOS group. The analysis was conducted under an air atmosphere from 35 to 700 °C at a heating rate of 10 °C min^{-1}.

3.6.4 X-Ray Diffraction

X-ray diffraction (XRD) was used to analyze the crystalline structure of the synthesized MOF powders and MOF-modified membranes. For membrane analysis, samples were cut into approximately 2 cm × 2 cm pieces and dried in an oven at 60 °C. MOF powder samples were analyzed after drying and grinding. XRD patterns were recorded using a Panalytical Empyrean diffractometer (Malvern Panalytical, Netherlands) with Cu Kα radiation (λ = 0.154 nm), available at the MECANOS group.

3.6.5 Water Contact Angle

Water contact angle measurements were performed to evaluate membrane surface wettability. Membrane samples were cut into approximately 2 cm × 2 cm pieces and dried at 60 °C before testing. A water droplet was placed on the membrane surface, and the contact angle was measured at two different points for each sample using an Attension Theta Lite optical tensiometer (Biolin Scientific, Sweden) that is available at the MECANOS group.

3.7 Pure water flux screening in Zaragoza

Preliminary pure water flux screening was conducted in Zaragoza to evaluate whether the fabricated TFN membranes had measurable hydraulic performance before further testing in Lund. The tests were performed using a stainless-steel Sterlitech HP4750 dead-end membrane module (Sterlitech Corporation, USA), connected to a nitrogen gas cylinder as the pressure source. The applied pressure was controlled using a pressure regulator and monitored with a pressure gauge placed upstream of the module. A schematic representation of the setup is shown in Figure 3.1.

For each test, approximately 150 mL of deionized water was used as the feed, and circular membrane coupons with a diameter of approximately 1.5 cm were mounted in the module. Before data collection, the membrane was stabilized at 10 bar for approximately 30 min. The permeate was collected in a beaker and manually weighed every 2 min using a balance. The permeate flux was then calculated from the collected permeate mass, membrane area, and filtration time.

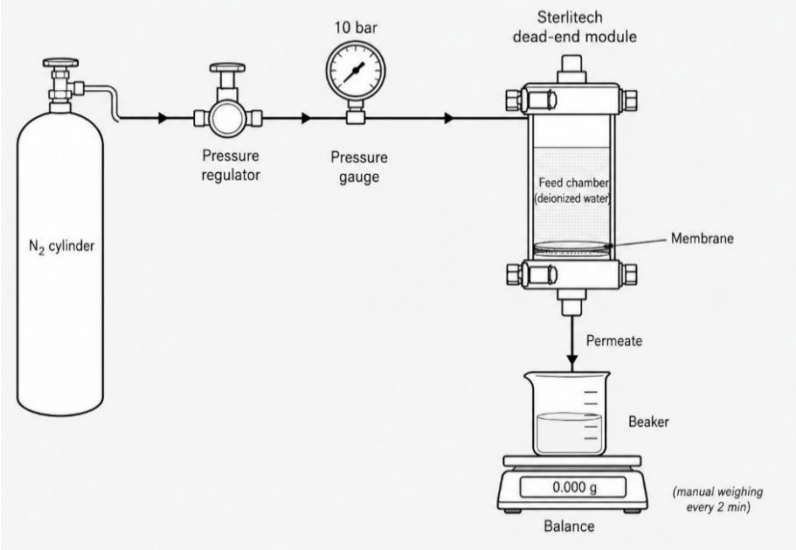

Figure 3.1 *Schematic representation of the Sterlitech dead-end filtration setup used for preliminary pure water flux screening in Zaragoza.*

3.8 Membrane filtration experiments in Lund

3.8.1 Membrane filtration setup

Pure water flux and PFAS filtration experiments were conducted at Lund University using the Bomberna crossflow filtration system. The system consisted of a 15 L feed tank, a pump, three flat-sheet membrane cell positions, pressure gauges, a flowmeter, permeate collection balances, and a computer-based data logging system. In this work, two membrane cells were used. Each cell had an effective membrane area of 1960 mm².

The feed solution was circulated from the feed tank to the membrane cells using a Hydra-Cell G10EPSGSFEHB pump (Wanner, USA), connected to a frequency converter (ELEX 4000, Bergkvist & Co. AB, Sweden) to control the flow rate. The two membrane cells were supplied with feed in parallel, and the retentate from each cell was returned to the feed tank. This configuration allowed crossflow operation across the membrane surface.

The temperature in the feed tank during cleaning was controlled using a temperature regulator (MCM-100, Shinko Technos Co., Ltd., Japan), a Pt100 temperature sensor (Pentronic, Sweden), and immersed electrical heaters. Feed and retentate pressures were monitored using pressure gauges connected to the system. These pressure values were used to calculate the transmembrane pressure (TMP). Permeate from each membrane cell was collected separately in beakers placed on electronic balances (PL6001-S, Mettler-Toledo AB, Sweden). The permeate mass was recorded every 30 s using NI LabVIEW 2020 software, which also calculated the permeate flux in real time. A schematic representation of the setup is shown in Figure 3.2.

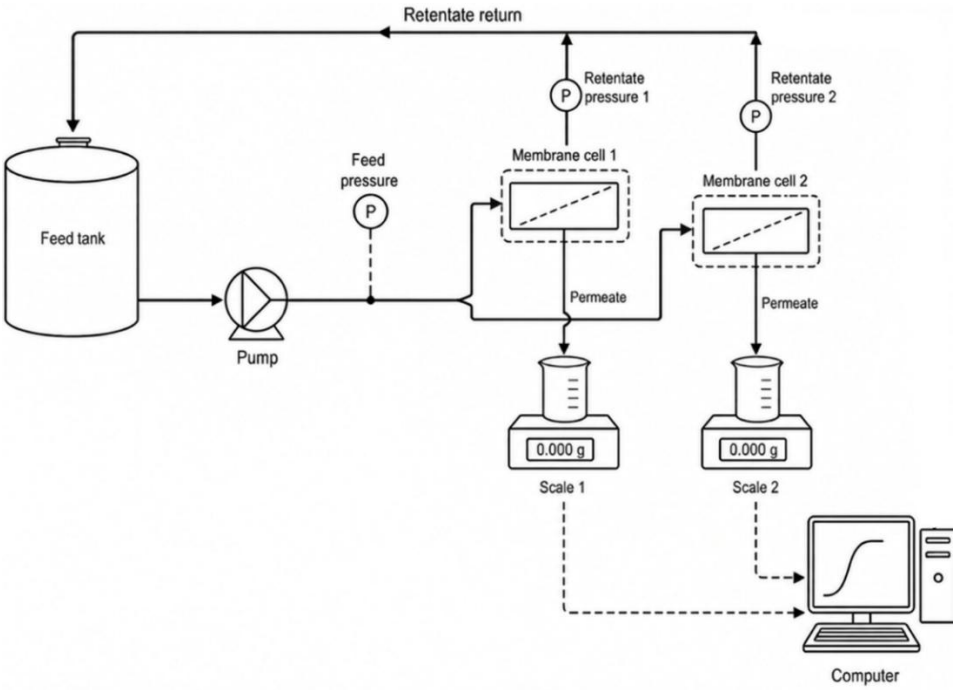

Figure 3.2 *Schematic representation of the crossflow membrane filtration system used at Lund University for pure water flux, PFAS filtration, and cleaning experiments.*

The membranes tested in Lund are summarized in Table 3.1, including the membrane type, MOF loading, and the corresponding filtration run.

Table 3.1 Membrane tested list and its filtration run

Filtration run	Sample placed in	
	Membrane cell 1	**Membrane cell 2**
1	PSf	PSf+PA
2	PSf+PA+UiO-66-NH_2 0.05%	PSf+PA+UiO-66-NH_2 0.1%
3	PSf+PA+ZIF-8 0.1%	PSf+PA+ZIF-8 0.2%

3.8.2 PFAS feed solution

The PFAS filtration experiments were performed using a standard PFAS spiking solution (FX19) prepared at the Swedish University of Agricultural Sciences (SLU) and sent to Lund University for the filtration tests. The spiking solution contained 15 PFAS compounds, covering perfluoroalkyl carboxylic and sulfonic acids with different carbon chain lengths. The stock solution contained 0.10 mg mL^{-1} of each PFAS compound. The detailed PFAS compounds included in the solution are listed in the appendix.

Before filtration, the PFAS feed solution was prepared by diluting the stock solution with deionized water to the target feed concentration. A total feed volume of 5 L was used for each PFAS filtration experiment.

3.8.3 Experimental procedure

The membrane filtration tests in Lund all followed the same procedure (Figure 3.3), which will be described in detail in each section below.

Figure 3.3 *Diagram representation of the experimental procedure that was done in Lund*

Before the initial pure water flux (PWF) measurement, each membrane was stabilized using deionized water. The system was operated at a TMP of 3 bar until permeate flow was established and the flux became stable. Stabilization continued for approximately 15 min after the first permeate drop appeared.

The initial pure water flux measurement, referred to as PWF 1, was then performed using deionized water at TMP values of 3, 4, and 5 bar. At each TMP, permeate mass was recorded for 10 min. After PWF 1, the feed was replaced with 5 L of PFAS-containing feed solution. PFAS filtration was conducted at a TMP of 10 bar for 1 h, and permeate mass was recorded continuously during the test. Feed and permeate samples were collected for subsequent PFAS analysis.

After PFAS filtration, the system was flushed with deionized water, and the pure water flux was measured again at TMP values of 3, 4, and 5 bar. This measurement was referred to as PWF 2. The membrane system was then cleaned by recirculating 10 L of 1 wt% Ultrasil 110 solution at 1 bar and 50 °C for 60 min. After cleaning, the system was flushed again with deionized water, and the final pure water flux measurement, referred to as PWF 3, was performed under the same TMP conditions as PWF 1 and PWF 2.

3.8.4 PFAS sample analysis

Feed and permeate samples collected during the PFAS filtration experiments were stored for chemical analysis. PFAS concentration analysis was planned to be performed after thesis submission by the responsible analytical group at SLU using liquid chromatography coupled with mass spectrometry. Therefore, PFAS rejection values were not available within the timeframe of this thesis.

3.9 Calculations

3.9.1 Permetae flux

The permeate flux for both pure water and PFAS filtration was calculated using Equation 1:

$$J = \frac{V}{A \times t} \tag{1}$$

where J is the flux (L m^{-2} h^{-1}), V is the collected permeate volume (L), A is the effective membrane area (m^2), and t is the filtration time (h).

3.9.2 Transmembrane pressure

For the crossflow experiments, TMP was calculated using Equation 2:

$$TMP = \frac{P_{in}+P_{out}}{2} - P_{permeate} \tag{2}$$

where P_{in} is the feed pressure, P_{out} is the retentate pressure, and $P_{permeate}$ is the permeate-side pressure. Since permeate was collected at atmospheric pressure, $P_{permeate}$ was considered approximately 0 bar.

3.9.3 Water permeability

Water permeability was obtained from the linear relationship between pure water flux and TMP in the range of 3-5 bar, as shown in Equation 3:

$$L_p = \frac{\Delta J}{\Delta TMP} \quad (3)$$

where L_p is the water permeability (L m^{-2} h^{-1} bar^{-1}), ΔJ is the change in pure water flux and ΔTMP is the corresponding change in transmembrane pressure.

3.9.4 Fouling factor

The fouling factor was calculated to evaluate the relative loss of water permeability after PFAS filtration. In this work, the fouling factor was calculated using water permeability instead of flux at a single TMP, because pure water flux was measured at several TMP values and converted into water permeability, as shown in Equation 4:

$$FF = \frac{L_{P1} - L_{P2}}{L_{P1}} \times 100 \quad (4)$$

where L_{P1} is the initial water permeability and L_{P2} is the water permeability after PFAS filtration. A higher (FF) indicates a larger permeability decrease after PFAS filtration.

3.9.5 Flux recovery ratio

The flux recovery ratio after cleaning was evaluated using Equation 5:

$$FRR = \frac{L_{P3}}{L_{P1}} \times 100 \quad (5)$$

where FRR is the flux recovery ratio (%), L_{P1} is the initial water permeability, and L_{P3} is the water permeability after cleaning.

4 Results and Discussion

4.1 Characterization of Synthesized MOFs

The synthesized MOF powders were investigated to determine their morphology, crystallinity, and chemical composition. This section focuses on MOF (ZIF-8, UiO-66-NH_2, and ZIF-94) characterization because these three MOFs were chosen for additional membrane evaluation and/or served as representative systems during initial screening.

SEM images of the synthesized MOF powders are presented in Fig. 4.1. Using ImageJ software, particle size distribution of each powder sample was determined by analyzing 50 randomly measured particles in an SEM image of each MOF system. As such, the error was expressed as the standard deviation. Average particle diameters for ZIF-8, UiO-66-NH_2, and ZIF-94 were found to be 59 ± 8 nm, 84 ± 17 nm, and 59 ± 9 nm, respectively. The reported values are larger than those reported in other studies for the same materials. Other researchers have reported that ZIF-8 and ZIF-94 nanoparticles had diameters of 30 ± 5 nm and 48 ± 8 nm, respectively (Refaat

et al., 2024) and that UiO-66-NH_2 particles made under equivalent reaction conditions ranged from about 43–59 nm (Pina-Vidal et al., 2024). Variations in synthesis scale, solvents, drying steps, and particle size determination via image processing may account for differences between the two sets of data.

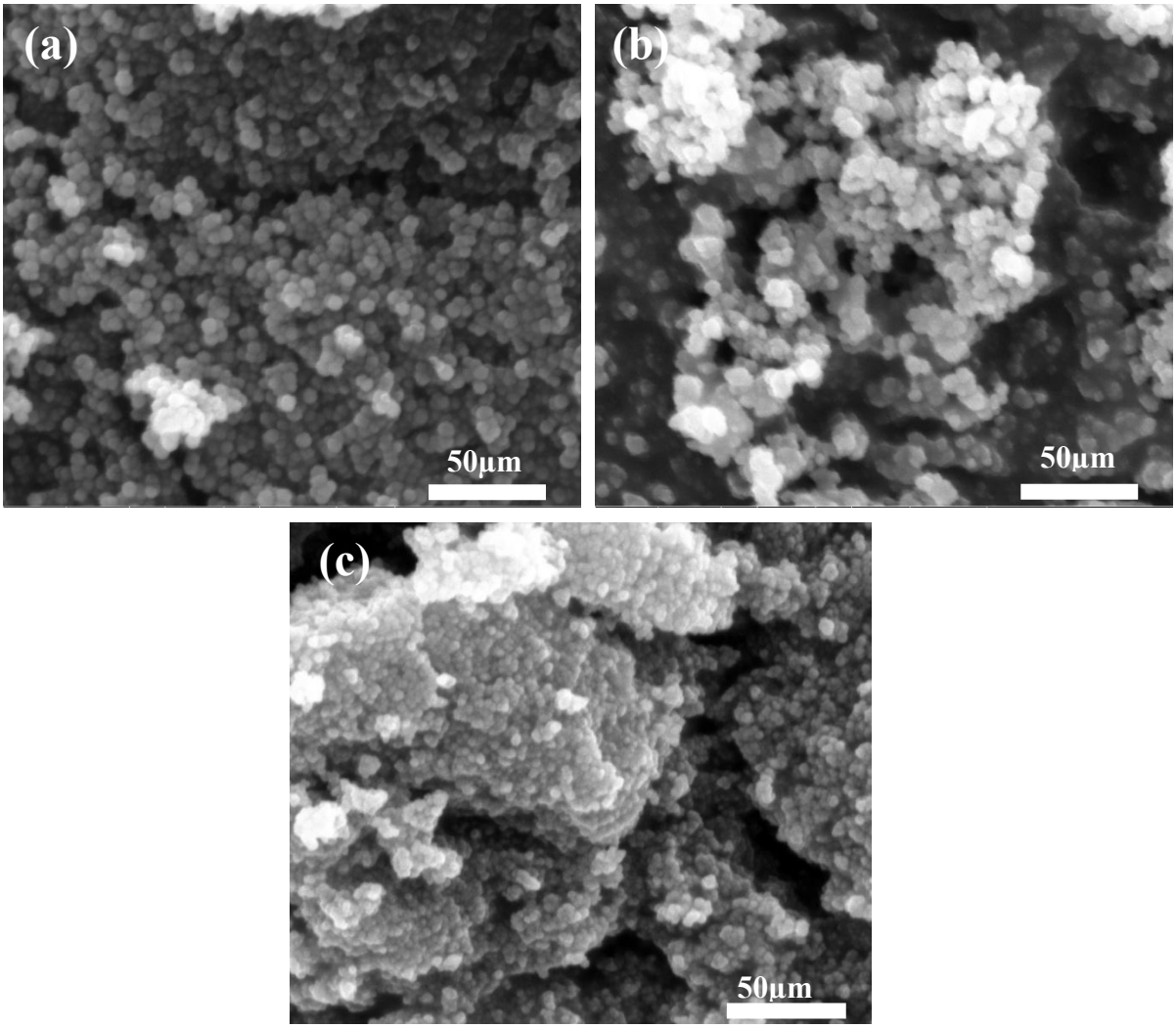

Figure 4.1 SEM images for MOFs that have been synthesized: (a). ZIF-8, (b). UiO-66-NH_2, (c). ZIF-94.

XRD (x-ray diffractometry) was employed to evaluate the degree of crystallinity of the three synthesized MOFs as pictured in Figure 4.2. The diffraction pattern of ZIF-8 and ZIF-94 shows characteristic peaks corresponding to zeolitic imidazolate frameworks reported in the literature (Martínez-Izquierdo et al., 2022; Refaat et al., 2024). Also, the pattern obtained for ZIF-94 provided evidence that the modification of ZIF-8 through solvent-assisted ligand exchange resulted in ZIF-94, as previously described (Martínez-Izquierdo et al., 2022). On the other hand, the diffractogram of UiO-66-NH_2 was indicative of a typical crystalline structure of zirconium-based UiO frameworks (Pina-Vidal et al., 2024), confirming the formation of the expected MOF phase. Therefore, overall, the XRD results indicated that all three synthesized powders retain crystalline MOF structures.

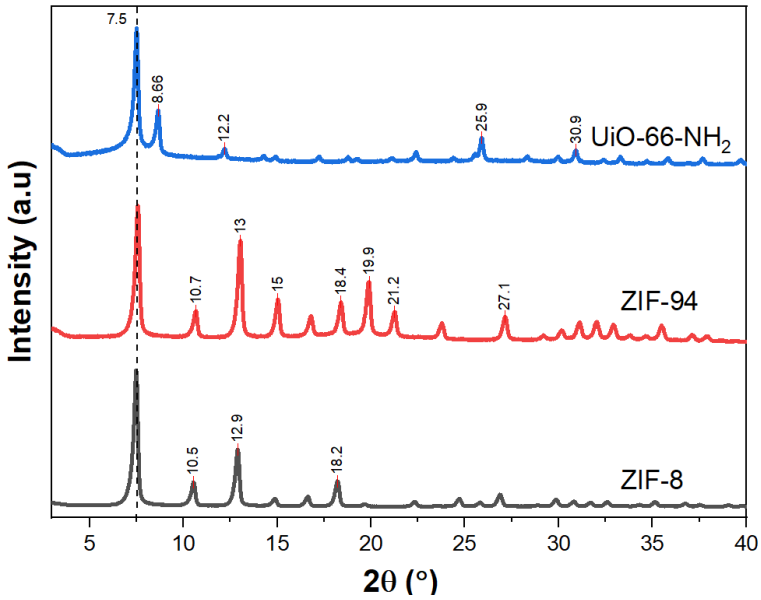

Figure 4.2 XRD patterns for MOFs.

Further structural information about the three MOFs was obtained through ATR-Fourier Transform Infrared Spectroscopy (ATR-FTIR). As depicted in Fig. 4.3, both ZIF-8 and ZIF-94 exhibited bands associated with imidazolate linkages. However, there was a shift to a lower wavenumber of a band related to a ZIF-8 linkage (near 993 cm^{-1}) for ZIF-94 due to changes in its ligand environment upon ligand substitution. In addition, ZIF-94 exhibited a strong band at ca. 1677 cm^{-1} assignable to C=O stretching from the aldehyde-containing ligands present in its precursor molecules, providing further evidence of the formation of ZIF-94 (Refaat et al., 2024).

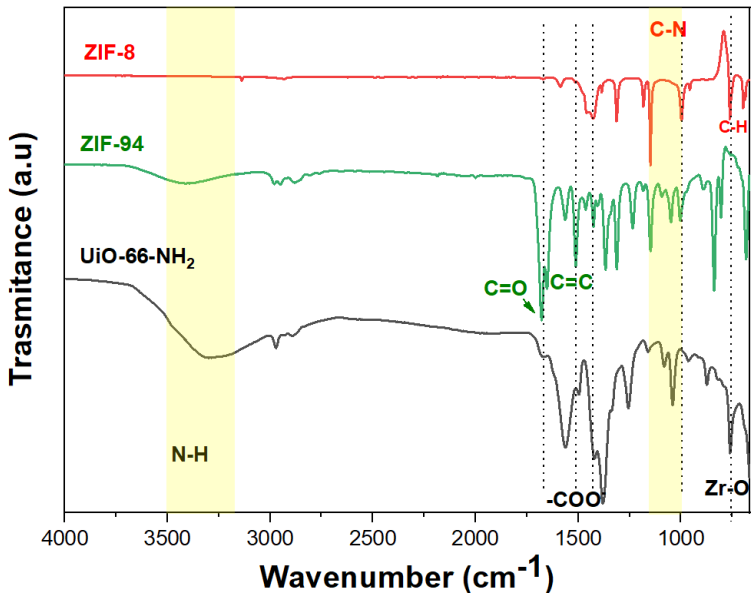

Figure 4.3 ATR-FTIR spectra for MOFs.

Finally, bands in the region between 3500–3300 cm^{-1} for UiO-66-NH_2 were attributed to NH2 groups, whereas bands centered at ca. 1430 cm^{-1} and 760 cm^{-1} were assigned to COO − groups bound to zirconium clusters and Zr-O vibrations, respectively (Aghajanzadeh et al.,

2018). Overall, these ATR-FTIR results provide confirmation of the successful preparation of the selected MOF powders and corroborate the findings derived from XRD measurements.

4.2 Morphology of TFC and TFN Membranes

The qualitative evaluation of membrane morphologies was carried out using SEM analysis. Due to differences in the availability of SEM images across different formulations, these images could not be directly used as a basis for an immediate quantitative comparison of selective layer thicknesses. Images of cross-sections of membranes were instead used to examine the development of a dense PA/MOF-containing upper region of each membrane, while surface images were used to determine if any visible MOF aggregation occurred and to assess surface heterogeneities.

4.2.1 Morphology of PSf support and PA-coated membrane

Fig. 4.4 compares the cross-sectionally evaluated morphology of the PSF support prior to coating with a PA layer and after it had been coated. Following interfacial polymerization, a much denser upper portion of the PSF support was observed, which indicated the presence of a PA layer. These observations are consistent with those typically found in TFC membranes. TFC membranes consist of a thin PA selective layer developed from interfacial polymerization reactions occurring between MPD and TMC on top of a porous substrate such as PSF (Petersen, 1993; Pham et al., 2021). In TFC membranes, the primary separation function occurs in the upper PA layer. The lower porous support serves to provide mechanical strength.

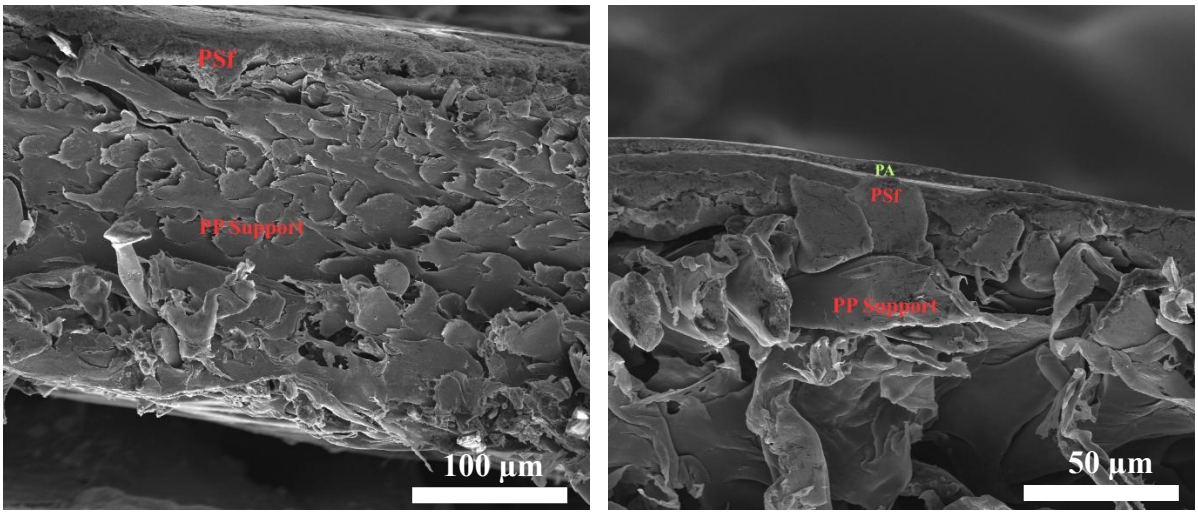

Figure 4.4: *Cross-section SEM pictures of PSf support vs PSf+PA.*

4.2.2 Effect of ZIF-8 loading on membrane morphology

Cross-sectional SEM images of the PSF + PA + ZIF-8 membranes prepared with ZIF-8 loadings of 0.05, 0.10, and 0.20% (w/v) are shown in Fig. 4.5. In all samples, a relatively compact upper region can be observed above the porous PSF support. However, the boundary between the PA/ZIF-8 selective layer and the PSF support is not sufficiently distinct to allow reliable identification or thickness measurement of the selective layer. Apparent differences in the upper-region thickness among the samples should therefore be interpreted with caution.

The ZIF-8 modified membranes generally demonstrated a significantly greater degree of homogeneity in the morphology of their upper layers compared to other MOF-modified membranes tested here. Based on this finding, it is likely that ZIF-8 was more compatible with the

reaction conditions required for forming a PA-based selective layer when preparing these membranes. Nonetheless, as noted previously, SEM cross-sectional images can also be influenced by local crack angles resulting from fracturing during specimen preparation and therefore represent only qualitative assessments of morphology.

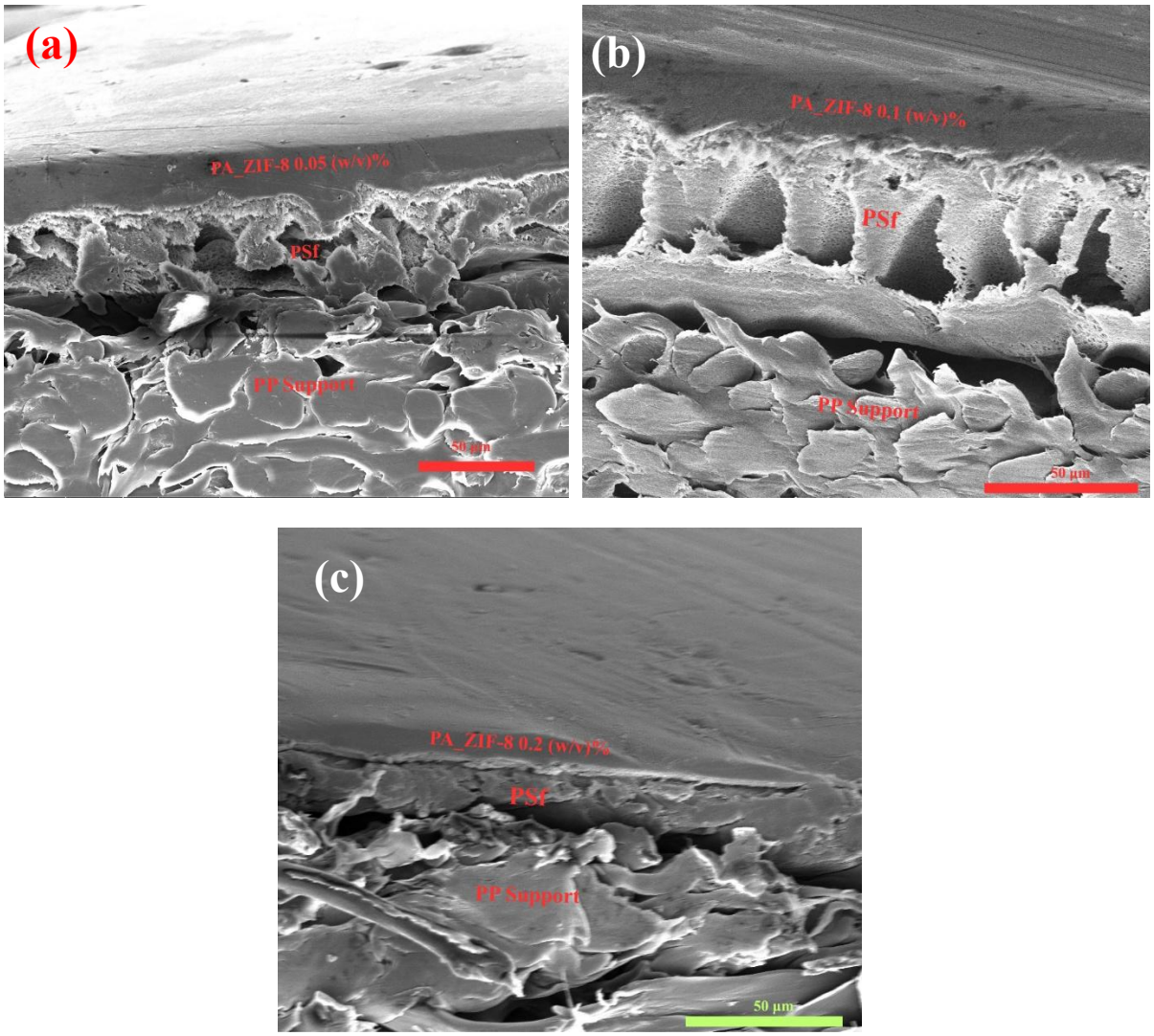

Figure 4.5 Cross-section SEM pictures of PSf+PA+ZIF-8: (a). 0.05 (w/v) %, (b). 0.1 (w/v) %, (c). 0.2 (w/)v %.

4.2.3 Effect of UiO-66-NH_2 loading on membrane morphology

Cross-sectional SEM images of PSF + PA + UiO-66-NH_2 membranes fabricated at 0.05%, 0.10%, and 0.20% w/v loading levels are presented in Fig. 4.6. As opposed to those observed for ZIF-8 modified membranes, significant particle agglomeration was evident in UiO-66-NH_2 modified membranes, especially at 0.10% and 0.20% loading levels. Notably, particle aggregation increased further at a loading level of 0.20%. Such findings suggest that higher concentrations of UiO-66-NH_2 may result in decreased stability of dispersions during membrane preparation.

MOF aggregation has implications regarding both the uniformity and selectivity of membranes with respect to nanofiltration applications. Well-dispersed nanofillers in TFN membranes can

improve water transport characteristics and surface properties; however, excessive aggregation can lead to non-uniform selective layers that either inhibit or enhance transport mechanisms, depending on their structural organization (Alam et al., 2026; Min et al., 2023). Thus, the observed aggregation of UiO-66-NH_2 particles via SEM imaging corresponds with the requirement to establish optimal MOF loading levels versus simply maximizing filler concentrations.

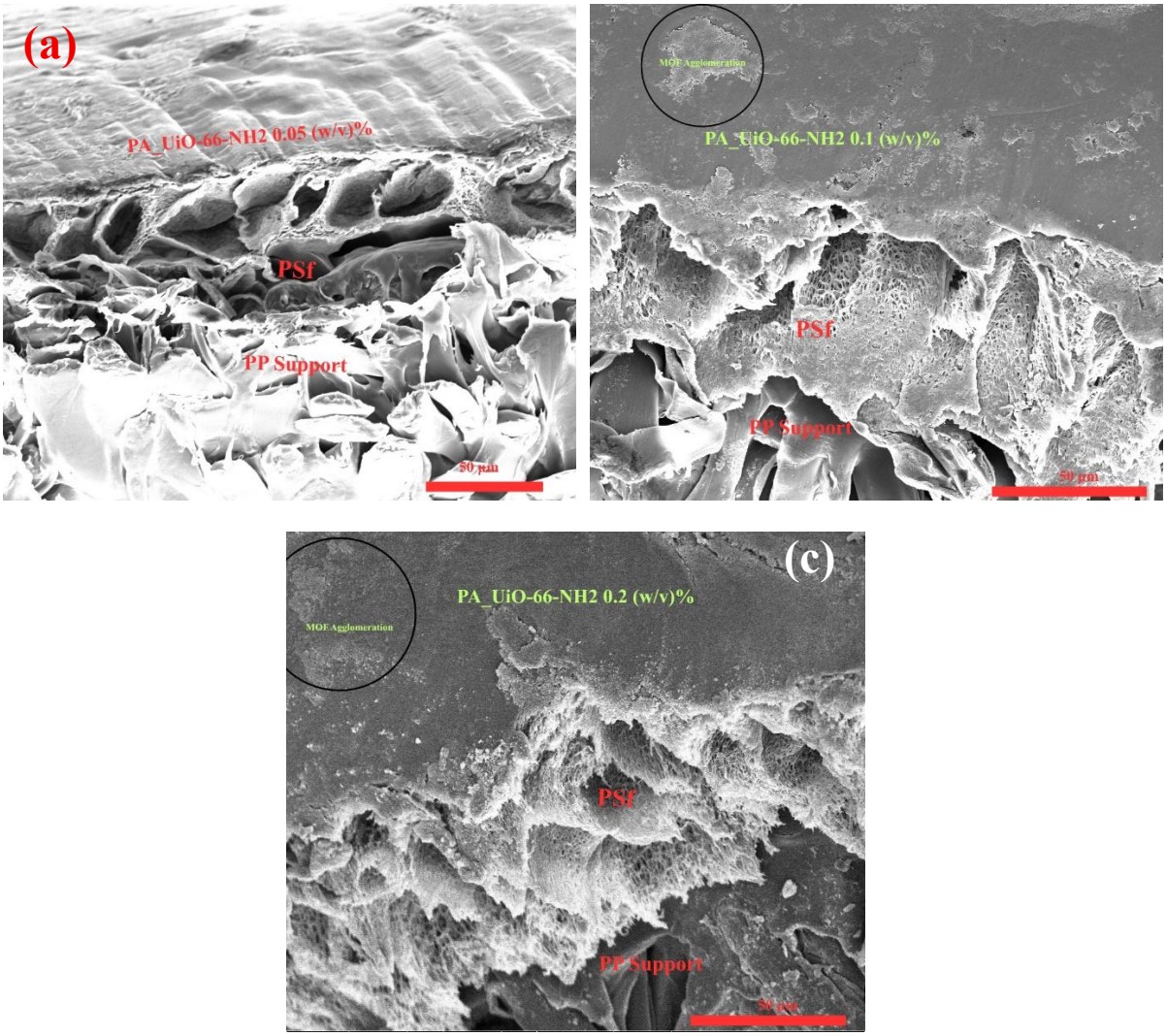

Figure 4.6 Cross-section SEM pictures of PSf+PA+UiO-66-NH_2: (a). 0.05 (w/v) %, (b). 0.1 (w/v) %, (c). 0.2 (w/v) %.

4.2.4 Morphology of ZIF-94 membrane

A representative cross-sectional SEM image of a 0.2% w/v loaded PSF + PA + ZIF-94 membrane is provided in Fig. 4.7. Comparison of this image with those obtained for ZIF-8 modified membranes indicates that the surface and upper layer morphology was less uniform for the ZIF-94 modified membrane. It may be inferred that the extent to which ZIF-94 particles become uniformly distributed throughout the selective layer may be reduced due to either less favorable particle dispersion conditions or enhanced local aggregation effects resulting from interfacial polymerization reactions involving ZIF-94. Given that this particular membrane was evaluated to exhibit low hydraulic performance during initial screening tests, the SEM image supports the inference that ZIF-94 is not suitable under the specified processing conditions utilized for fabricating these membranes.

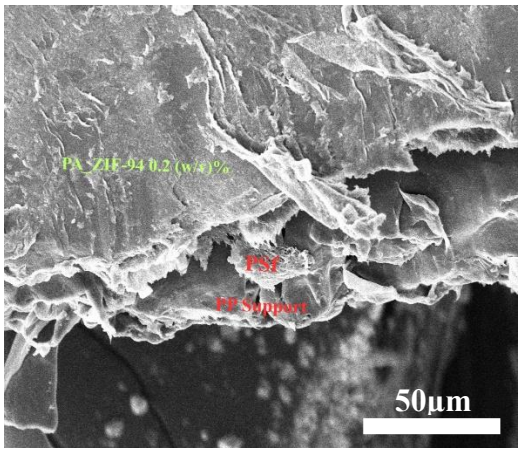

Figure 4.7 Cross-section SEM picture of PSf+PA+ZIF-94 0.2 (w/v) %.

4.3 Evidence of MOF Incorporation in the Polyamide Layer

4.3.1 Elemental evidence from EDX

SEM-EDX was conducted to examine the chemical composition of the surface of the membrane and to verify that the MOF particles were incorporated properly into the PA layer. The detailed measured area and the spectra are attached in the appendix. Palladium was present in the spectrum as a result of using palladium-coated carbon tape as a conductive film to prepare the samples for SEM analysis. The main components of carbon and oxygen were due to the PA/PSf membrane material. At the same time, the presence of the metal marker element served as proof that the MOFs had been successfully added.

Key elements detected via EDX are presented in Table 4.1. The presence of zinc was detected in both PSf+PA+ZIF-8 and PSf+PA+ZIF-94 membranes, consistent with the Zn-based structure of the respective ZIFs. The detection of zirconium within the UiO-66-NH_2 modified membranes verified the existence of the Zr-based MOF. It is important to note that the metal content levels detected via EDX were low. Since the MOF loadings employed throughout this work ranged from 0.1-0.2% (w/v), it would therefore be appropriate to interpret EDX as providing either qualitative or semi-quantitative evidence of MOF addition rather than an accurate measure of filler loading.

Table 4.1: Key elements detected by EDX.

Sample	Important marker element (Wt%)			
	C	O	Zn	Zr
PSf+PA+ZIF-8 0.1%	63.54	12.72	1.30	-
PSf+PA+ZIF-8 0.2%	60.52	18.37	1.27	-
PSf+PA+UiO-66-NH_2 0.1%	68.71	18.24	-	1.67
PSf+PA+UiO-66-NH_2 0.2%	66.11	17.82	-	2.22
PSf+PA+ZIF-94 0.2%	73.91	9.31	0.69	-

The weight percentage of Zr present increased from 1.67 wt % for UiO-66-NH_2 at 0.1% to 2.22 wt % for UiO-66-NH_2 at 0.2%, which indicates a correlation to the increase in MOF loading. Conversely, the amount of Zn found in the ZIF-8 membranes did not differ based on the MOF

loadings of 0.1% and 0.2%. Possible localized heterogeneities of the measured region, or differences in how particles were dispersed throughout the membrane, may explain the similarities observed at 0.1% and 0.2% MOF loadings. This illustrates a limitation of EDX when measuring very low-load TFN membranes, wherein the detected chemistry will depend greatly on what part of the membrane's surface is chosen for analysis.

4.3.2 FTIR analysis of membranes

Figure 4.8 shows the FTIR spectra of PSf, PSf+PA, and selected TFN membranes containing ZIF-8, UiO-66-NH_2, and ZIF-94 at 0.2% (w/v). Overall, the spectra of the membranes were similar because the signal was dominated by the polymer matrix, especially PSf and the PA selective layer. This is expected for low MOF loadings, where filler-related bands may be weak or overlapped with polymer absorption bands.

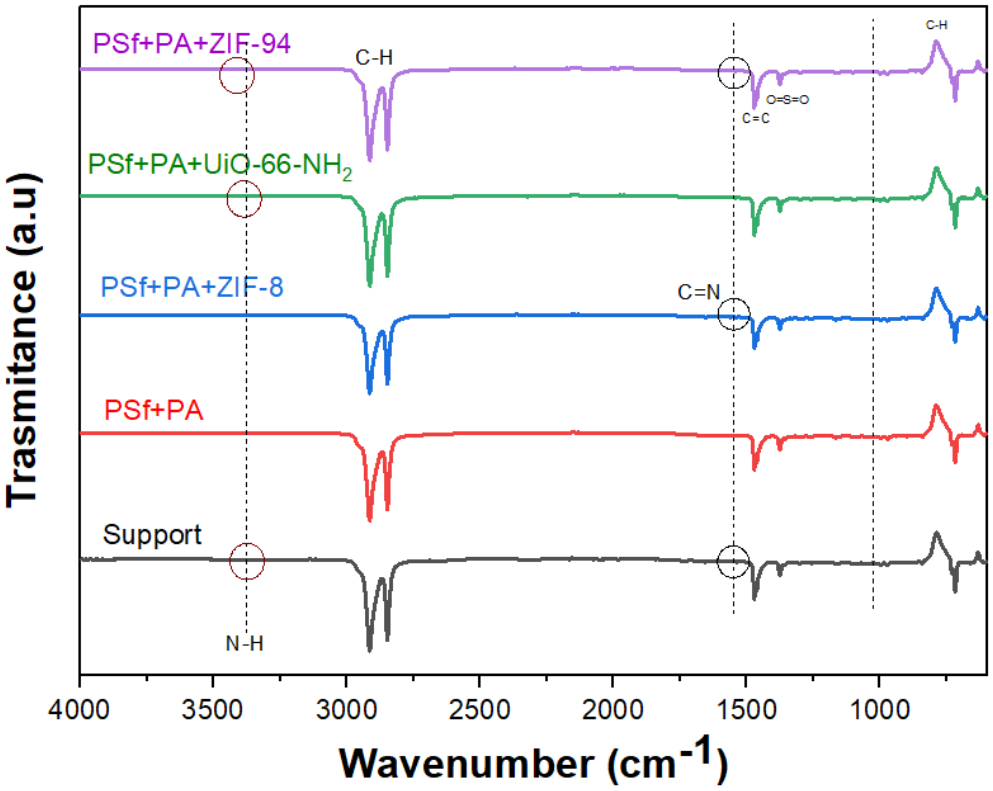

Figure 4.8 FTIR membranes overlay for: PSf, PSf+PA, ZIF-8 0.2(w/v)%, UiO-66-NH_2 0.2(w/v)%, ZIF-94 0.2(w/v)%.

The formation of the PA layer can be supported by the presence of amide-related bands. Aromatic MPD–TMC polyamide membranes typically show amide I and amide II bands around 1660 and 1540 cm^{-1}, along with aromatic amide-related bands near 1610 cm^{-1} (Idarraga-Mora et al., 2019). In the TFN membranes, small changes or shoulders were observed in regions associated with MOF functional groups. For UiO-66-NH_2, the broad region around 3300–3500 cm^{-1} may be related to N–H stretching from amino groups, while the Zr–O and carboxylate-related vibrations are expected at lower wavenumbers (Aghajanzadeh et al., 2018; Pina-Vidal et al., 2024). For ZIF-based membranes, bands near 1580 cm^{-1} can be associated with C=N stretching from imidazolate ligands (Refaat et al., 2024; Thompson et al., 2013).

However, because the MOF loading was low and the spectra were dominated by the polymer matrix, FTIR alone cannot be used as definitive evidence of MOF incorporation. Instead, the FTIR spectra provide complementary support when interpreted together with EDX and XRD results.

4.3.3 XRD analysis of membranes

Figure 4.9 shows the XRD data for the TFN membranes, which showed significantly lower levels of MOF-related peaks than those found in the corresponding powder forms of MOF shown in Figure 4.2. This result can be attributed to a very low level of MOF within the membranes, thus causing the diffraction signal generated from the membranes to be primarily influenced by the PA/polymer matrix. At first glance, the ZIF-8 and ZIF-94 modified membranes appear to be quite similar to the PA membrane; however, some peaks associated with the MOF powders appear, especially in areas of the spectrum that would correspond to peaks associated with the respective MOF powders. These effects are believed to arise due to low filler content (i.e., low MOF loading), interactions between the MOF and polymer matrix, as well as environmental changes resulting from being embedded into the PA layer.

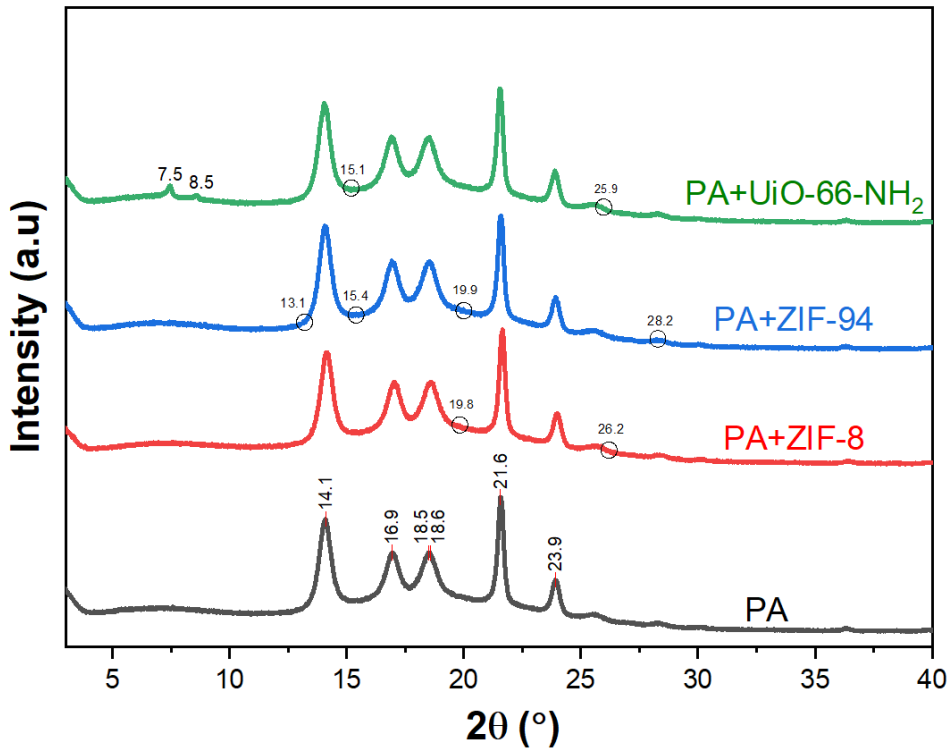

Figure 4.9 XRD membrane patterns for: PSf+PA, ZIF-8 0.2 (w/v)%, UiO-66-NH₂ 0.2 (w/v)%, ZIF-94 0.2(w/v)%.

Among the three TFN membranes, the UiO-66-NH₂-modified membrane showed the clearest MOF-related peaks. This is consistent with the SEM observations, where UiO-66-NH₂ aggregation was more visible. Local MOF-rich regions may increase the intensity of crystalline reflections. In contrast, ZIF-8 and ZIF-94 showed only minor peaks, suggesting that their crystalline signals were present but weak within the membrane matrix.

4.4 Surface Wettability of MOF-Modified Membranes

The surface wettability of each of the membranes was determined through measurement of their water contact angles. The contact angle for the PSf+PA membrane, as shown in Figure 4.10, was found to be approximately 50.5° ± 1.4°, indicating a hydrophilic nature. Because all the measured contact angles were under 90°, it can be concluded that all of the surfaces tested are hydrophilic. The degree of hydrophilicity varied depending on the type of MOF used, as shown in Figure 4.10.

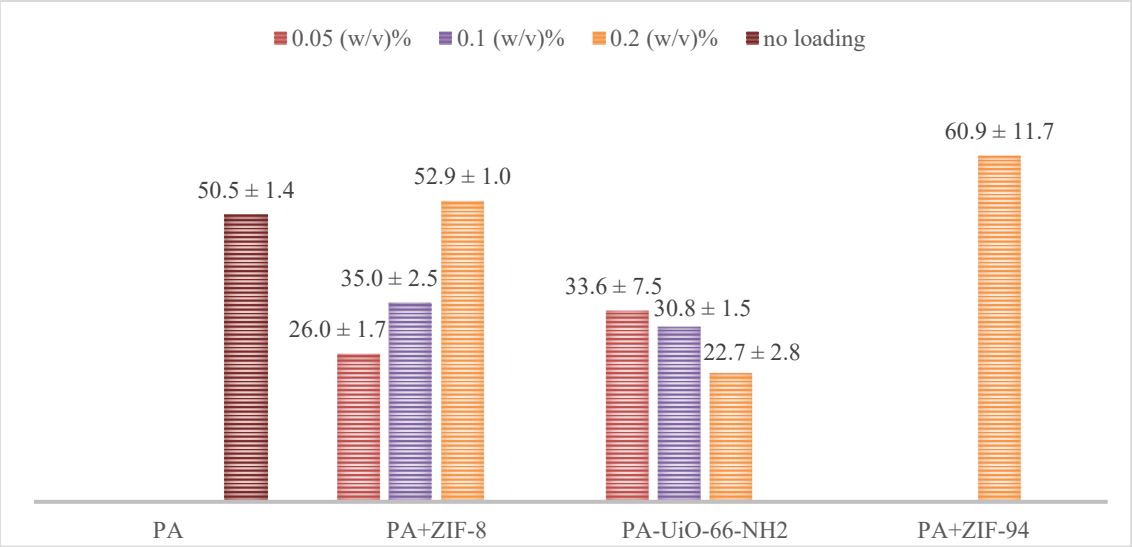

Figure 4.10 Bar chart of WCA (the number present in ˚).

Contact angle measurements for membrane surfaces containing ZIF-8 indicated an increase in contact angles as a function of increasing loading levels (From 0.05% to 0.2%). The contact angles for these samples were approximately 26.0° ± 1.7° and 52.9° ± 1.0°, respectively. It is likely that the observed effect of MOF concentration on contact angle is due to the inherent hydrophobic characteristics of ZIF-8, which includes both methylimidazole linkers and has been identified in prior research studies to be one of the most hydrophobic forms of ZIFs (Refaat et al., 2024, Park et al., 2006).

On the other hand, when contact angle measurements were taken for samples containing UiO-66-NH_2, they indicated a decrease in contact angle as a function of increasing MOF loading levels. Specifically, as the loading level of UiO-66-NH_2 was increased from 0.05% to 0.2%, the contact angle decreased from 33.6° ± 7.5° to 22.7° ± 2.8°. These data are indicative of an increasingly hydrophilic surface with increasing UiO-66-NH_2 loading. This observation is consistent with the properties of UiO-66-NH_2, including its Zr-Oxide cluster and amine functional groups, which contribute to its ability to interact with and attract water molecules.

ZIF-94 had the highest contact angle (approximately 60.9° ± 11.7°) and therefore exhibited the lowest degree of hydrophilicity of any membrane tested using TFN. In addition to having the largest standard error, these results suggest that there exists considerable surface heterogeneity within these films, which is consistent with observations made during SEM analysis.

Therefore, based upon these findings, it appears that the type of MOF used will have a significant impact on the degree of hydrophilicity present at the surface of each film. Each property

is important as well because it affects water transport, fouling tendency, and interactions with dissolved solutes.

4.5 Thermal Stability of Membranes

Figure 4.11 presents the TGA curves of the PSf support, PSf+PA membrane, and selected TFN membranes containing UiO-66-NH_2 and ZIF-8. The PSf support showed gradual weight loss at lower temperature, followed by major degradation between approximately 300 and 500 °C. After PA formation, the PSf+PA membrane remained stable up to around 250 °C before undergoing its main degradation step.

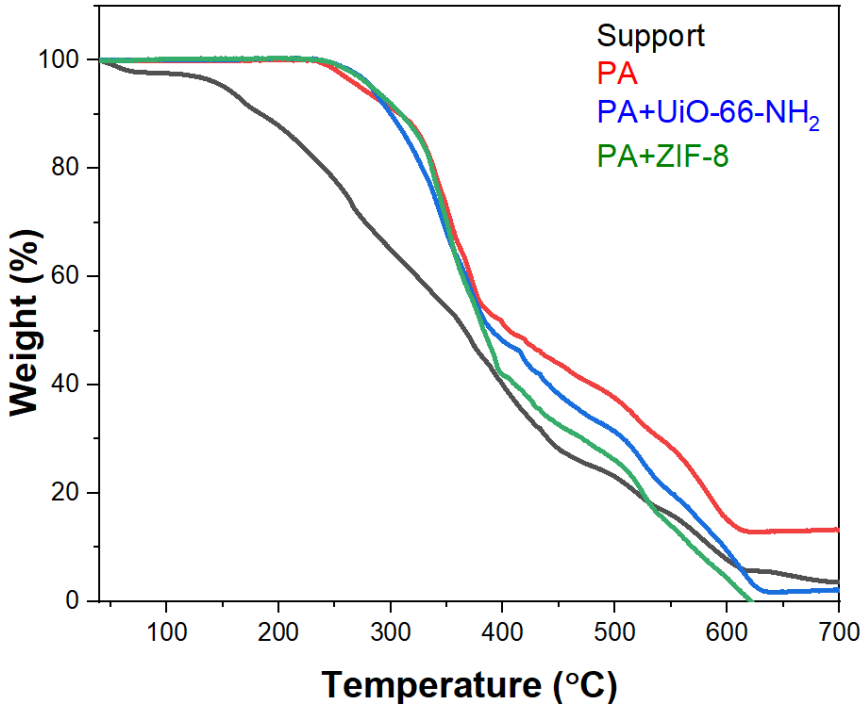

Figure 4.11 TGA results for support, PA, PA+UiO-66-NH_2, and PA+ZIF-8 membranes.

The UiO-66-NH_2- and ZIF-8-modified membranes showed degradation profiles broadly similar to the PSf+PA membrane, indicating that the low MOF loading did not strongly alter the overall thermal stability of the membranes. Minor differences between the curves may be related to MOF incorporation and local differences in the PA/MOF layer, although the thermal response was mainly dominated by the polymeric membrane matrix.

Overall, the TGA results confirm that the prepared membranes were thermally stable within the temperature range relevant for the filtration experiments, which were performed far below the main degradation region.

4.6 Membrane Permeability

Based on the preliminary pure water flux screening in Zaragoza and the limited experimental time available in Lund, six membranes were selected for crossflow filtration testing: the PSf support, PSf+PA, UiO-66-NH_2 0.05%, UiO-66-NH_2 0.1%, ZIF-8 0.1%, and ZIF-8 0.2%. The detailed preliminary screening results are provided in the Appendix.

The hydraulic performance of the selected membranes was evaluated from pure water permeability measurements before PFAS filtration, after PFAS filtration, and after cleaning. These values are denoted as (L_p 1), (L_p 2), and (L_p 3), respectively. Water permeability was calculated from the pure water flux measured at TMP values of 3, 4, and 5 bar using Eq. (3). The fouling factor and flux recovery ratio were calculated using Eq. (4) and Eq. (5), respectively. The resulting values are presented in Figures 4.12 and 4.14.

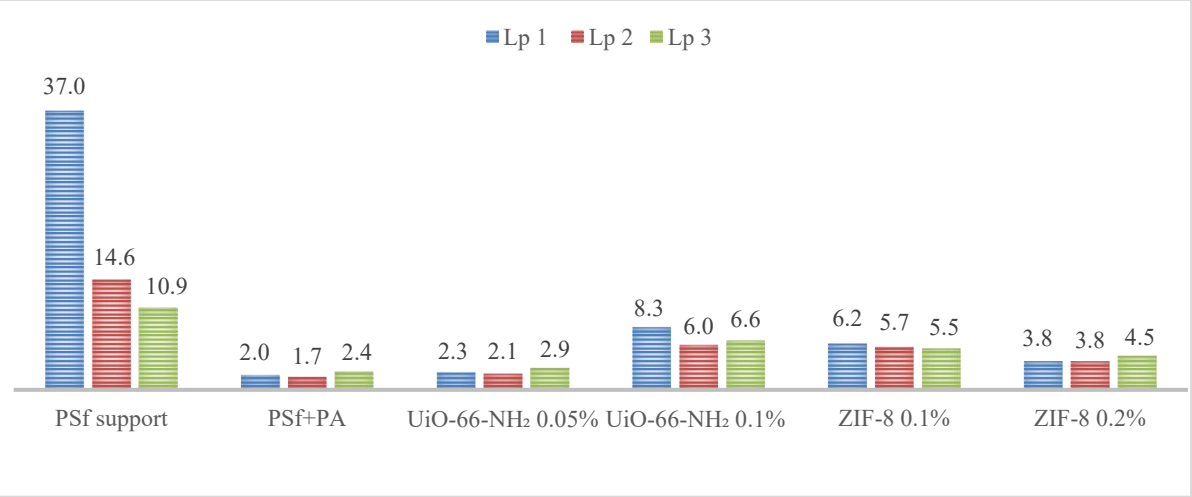

Figure 4.12 Water permeability before PFAS filtration or initial (Lp 1), after PFAS filtration (Lp 2), and after cleaning (Lp 3). Water permeability is reported in LMH/bar.

The PSf support showed the highest initial permeability, with L_{p1} of 37.0 LMH bar^{-1}. This was expected because the commercial PSf support is a porous support membrane and does not contain a dense polyamide selective layer. Therefore, it was used as a hydraulic reference rather than as a membrane expected to provide high PFAS rejection. After interfacial polymerization, the permeability decreased strongly to 2.0 LMH bar^{-1} for the PSf+PA membrane. This decrease confirms that the formation of the PA selective layer introduced additional resistance to water transport.

Among the PA-coated membranes, UiO-66-NH_2 0.1% showed the highest initial permeability, with L_{p1} of 8.3 LMH bar^{-1}, followed by ZIF-8 0.1% with 6.2 LMH bar^{-1}. Both values were higher than that of the unmodified PSf+PA membrane, indicating that MOF incorporation can improve water transport through the PA selective layer when the filler type and loading are suitable. Previous studies have also reported that porous fillers can improve membrane permeance when they are well distributed within the selective layer, as they may provide additional pathways for water transport (Bi et al., 2024; Refaat et al., 2024). However, this effect strongly depends on filler dispersion and compatibility with the polyamide matrix. Excessive loading or local aggregation can instead introduce additional transport resistance or create non-uniform selective layers (Bi et al., 2024).

However, the high permeability of UiO-66-NH_2 0.1% should be interpreted with caution. As shown in Figure 4.13, visible defects were observed on the UiO-66-NH_2-modified membranes. This suggests that the increased permeability may not only originate from improved water transport through the MOF-modified PA layer, but may also be partly related to imperfections

in the selective layer. In nanofiltration membranes, such defects can increase water flux but may compromise selectivity.

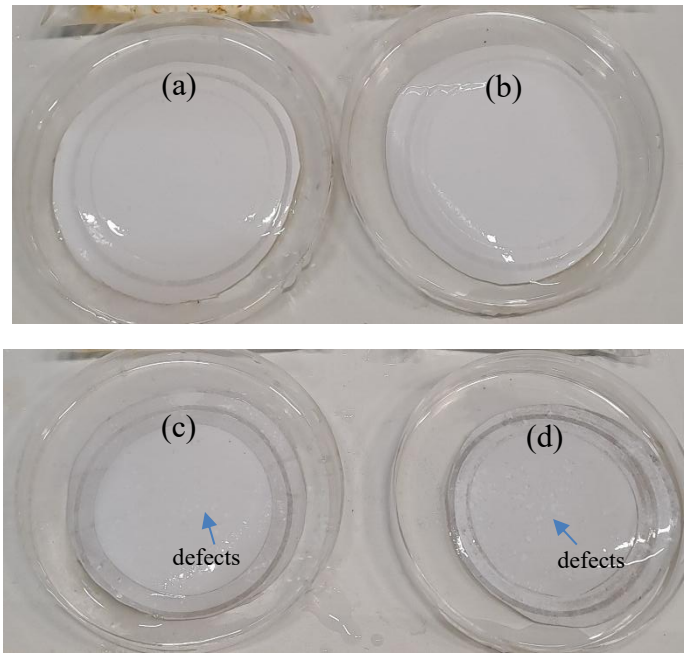

Figure 4.13 Picture of membrane after filtration:(a)ZIF-8 0.1%, (b)ZIF-8 0.2%, (c)UiO-66-NH_2 0.05%, (d) UiO-66-NH_2 0.1%.

In the ZIF-8 series, increasing the loading from 0.1% to 0.2% decreased L_{p1} from 6.2 to 3.8 LMH bar^{-1}. This suggests that the beneficial effect of ZIF-8 was not simply proportional to loading. At higher loading, additional particles may increase transport resistance or introduce local heterogeneity in the selective layer. Although macroscopic defect observation was less conclusive for the ZIF-8 membranes due to their more transparent appearance, the SEM images showed a more homogeneous morphology than that observed for UiO-66-NH_2-modified membranes.

The fouling factor was used to evaluate the relative decrease in permeability after PFAS filtration. As shown in Figure 4.14, the PSf support showed the highest fouling factor, 60.5%, indicating a strong loss of hydraulic performance after PFAS filtration. In contrast, the PSf+PA membrane showed a much lower fouling factor of 12.7%, suggesting that the PA layer improved hydraulic stability compared with the uncoated support.

The ZIF-8-modified membranes showed the lowest fouling factors among the PA-coated membranes, with values of 8.1% for ZIF-8 0.1% and 0.8% for ZIF-8 0.2%. This indicates that both ZIF-8-modified membranes retained most of their permeability after PFAS filtration. For UiO-66-NH_2, the 0.05% membrane also showed a low fouling factor of 8.1%, while the 0.1% membrane showed a higher value of 28.0%. Although UiO-66-NH_2 0.1% had the highest initial permeability, its larger permeability decrease after PFAS filtration and the visible defects shown in Figure 4.13 indicate that its hydraulic performance should not be interpreted as purely beneficial without PFAS rejection data.

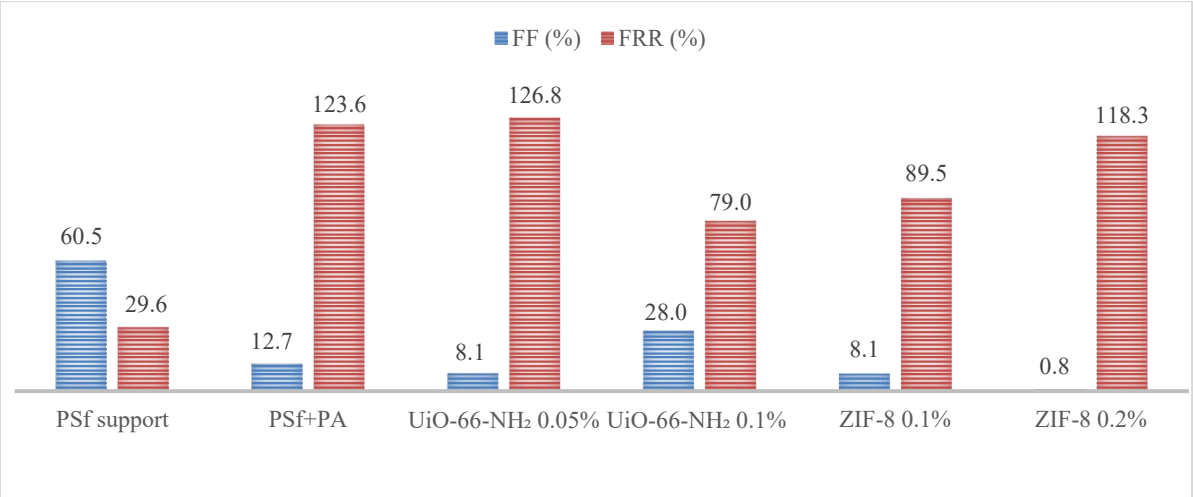

Figure 4.14 FF and FRR data of the membranes.

After cleaning, the hydraulic recovery was evaluated using the flux recovery ratio. The PSf support showed poor recovery, with an FRR of 29.6%, indicating that its permeability was not restored after cleaning. In contrast, the PSf+PA, UiO-66-NH_2 0.05%, and ZIF-8 0.2% membranes showed FRR values above 100%. These values should be interpreted carefully, as they do not necessarily indicate permanent improvement in membrane performance. They may instead be related to additional membrane conditioning during operation, membrane relaxation, or changes induced by the cleaning step. The ZIF-8 0.1% membrane showed an FRR of 89.5%, meaning that most of its initial permeability was recovered after cleaning.

Overall, the permeability results show that MOF incorporation can improve the hydraulic performance of PA-coated membranes, but the effect depends strongly on MOF type, loading, and membrane integrity. UiO-66-NH_2 0.1% provided the highest initial permeability, but the presence of visible defects and the higher fouling factor make this result less straightforward to interpret. In comparison, ZIF-8 0.1% showed a more balanced performance, combining relatively high permeability, low fouling factor, good hydraulic recovery, and more homogeneous morphology. Therefore, ZIF-8 0.1% was considered the most promising formulation from the hydraulic performance results, although final confirmation of its suitability for PFAS removal requires rejection analysis.

4.7 PFAS Filtration

The permeate flux during PFAS filtration was measured at a TMP of 10 bar for the six membranes tested in the Lund crossflow system. The results are shown in Figure 4.15. Since the PFAS concentration analysis was not available within the timeframe of this thesis, this section focuses only on the hydraulic behavior of the membranes during PFAS filtration. Final evaluation of PFAS removal will require the feed and permeate concentration data.

The PSf support showed the highest PFAS filtration flux, with a value of 225.0 LMH. This result was expected because the commercial PSf support is a porous support membrane with a much larger MWCO than the PA-coated membranes. Therefore, it should only be used as a

hydraulic reference and not as a fair comparison for PFAS rejection performance. The unmodified PSf+PA membrane showed a much lower PFAS flux of 19.0 LMH, confirming the additional resistance introduced by the PA selective layer.

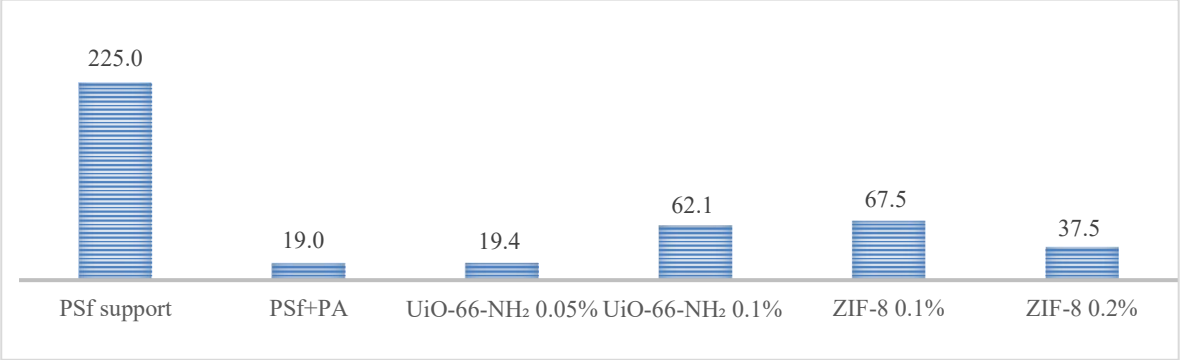

Figure 4.15. PFAS permeate flux at 10 bar. Flux is reported in LMH.

Among the PA-coated membranes, ZIF-8 0.1% showed the highest PFAS filtration flux, 67.5 LMH, followed by UiO-66-NH_2 0.1% with 62.1 LMH. Both values were substantially higher than the flux of the unmodified PSf+PA membrane, suggesting that MOF incorporation can improve water transport during PFAS filtration when the filler type and loading are suitable. However, as discussed in Section 4.6, the high flux of UiO-66-NH_2 0.1% should be interpreted carefully because visible defects and particle aggregation were observed for UiO-66-NH_2-modified membranes. These imperfections may contribute to higher flux, but they may also reduce membrane selectivity.

The ZIF-8 series showed a clear dependence on MOF loading. The ZIF-8 0.1% membrane gave the highest PFAS filtration flux, while increasing the loading to 0.2% reduced the flux to 37.5 LMH. This suggests that 0.1% ZIF-8 provided a more favorable balance between improved water transport and selective-layer integrity. At higher loading, the additional particles may have increased transport resistance or introduced local heterogeneity in the PA layer.

The PFAS filtration fluxes obtained in this work can also be compared cautiously with the commercial membrane study by Kakati (2024), who tested commercial NF and RO membranes using the same FX19 PFAS spiking solution. In that study, commercial NF membranes generally showed higher permeate fluxes than the TFN membranes prepared in this work, with NF99HF and NF270 showing particularly high fluxes under the tested conditions. Commercial RO membranes also showed high fluxes, especially BW30, although they were operated at a higher pressure. However, this comparison should be interpreted carefully because the commercial membranes were tested in a different membrane system, with different membrane area, operating pressure, recovery, and hydrodynamic conditions.

Overall, the PFAS filtration results indicate that MOF incorporation improved the hydraulic performance of the PA-coated membranes, but the improvement depended strongly on MOF type and loading. ZIF-8 0.1% showed the most promising hydraulic behavior during PFAS filtration because it combined the highest PFAS filtration flux among the PA-coated membranes with low fouling factor and more homogeneous morphology. Nevertheless, its suitability for PFAS removal can only be confirmed after PFAS rejection analysis.

5 Conclusions

This thesis explored the development of MOF-modified thin-film nanocomposite membranes as a potential approach for PFAS removal from drinking water. The work focused on understanding how different MOF fillers influence membrane formation, surface properties, and hydraulic performance when incorporated into a polyamide selective layer.

Five MOFs were considered in this study: ZIF-8, ZIF-L, ZIF-94, NH_2-ZIF-8, and UiO-66-NH_2. After synthesis and initial characterization, these materials were evaluated as possible fillers in TFN membranes prepared by interfacial polymerization on commercial polysulfone support. The preliminary pure water flux screening showed that not all MOFs produced hydraulically workable membranes. ZIF-L and NH_2-ZIF-8 resulted in membranes with no measurable flux, while ZIF-94 showed very low hydraulic performance. Based on this screening and the limited experimental time available, ZIF-8- and UiO-66-NH_2-modified membranes were selected for further evaluation in Lund.

The characterization results showed that MOF incorporation affected membrane structure and surface properties in different ways. SEM images suggested that ZIF-8 produced a relatively more homogeneous membrane morphology, whereas UiO-66-NH_2 showed visible particle aggregation, especially at higher loading. Visual inspection also indicated defects in UiO-66-NH_2-modified membranes, which should be considered when interpreting their high permeability. EDX analysis supported the presence of MOFs in the membranes through the detection of Zn in ZIF-based membranes and Zr in UiO-66-NH_2-modified membranes. FTIR and XRD provided complementary evidence, although the MOF-related signals in the membranes were weak due to the low filler loading and the dominant polymer matrix.

The water contact angle results showed that the effect of MOF addition depended strongly on the framework type. ZIF-8 tended to increase the contact angle at higher loading, suggesting a less hydrophilic surface, while UiO-66-NH_2 showed the opposite trend and increased membrane hydrophilicity. These results confirm that MOF chemistry and functional groups play an important role in determining the surface properties of the polyamide selective layer.

The filtration results showed that MOF incorporation can improve membrane hydraulic performance, but only when the MOF type, loading, and membrane integrity are suitable. UiO-66-NH_2 0.1% showed the highest initial water permeability among the PA-coated membranes. However, this result should be interpreted with caution because visible defects and aggregation were observed, meaning that the high flux may not only originate from improved transport through the MOF-modified polyamide layer. In contrast, ZIF-8 0.1% showed a more balanced performance, combining relatively high water permeability, low fouling factor, good hydraulic recovery, high PFAS filtration flux at 10 bar, and more homogeneous morphology.

Overall, this work shows that MOF-modified TFN membranes are a promising route for improving the hydraulic performance of polyamide nanofiltration membranes. However, MOF incorporation is not automatically beneficial. The final membrane performance depended strongly on MOF type, loading, dispersion quality, and the integrity of the selective layer. In this study, ZIF-8 at 0.1% (w/v) appeared to provide the best overall balance between morphology, permeability, fouling resistance, and filtration flux. Nevertheless, the actual PFAS removal performance still needs to be confirmed once PFAS concentration analysis of the feed and permeate samples is available.

6 Future Work

The most immediate future step is to analyse the PFAS concentrations in the feed and permeate samples collected during filtration. These results are needed to calculate the actual PFAS rejection and to determine whether the improved flux observed for some MOF-modified membranes is also accompanied by effective PFAS removal. This will be especially important for comparing long-chain and short-chain PFAS, since they may behave differently during nanofiltration.

Further work should also optimize the MOF loading and dispersion. In this thesis, ZIF-8 at 0.1% (w/v) showed the most balanced hydraulic performance, while 0.2% (w/v) resulted in lower flux. Therefore, future studies could focus on narrower loading ranges around this value. For UiO-66-NH_2, the main challenge was particle aggregation and visible defect formation. Improving dispersion through optimized sonication, solvent compatibility, particle pretreatment, or surface modification could help produce more uniform selective layers.

Reproducibility should be tested more carefully in future experiments. Duplicate or triplicate fabrication and filtration tests are needed to confirm whether the observed trends are consistent, since MOF dispersion and local defects can strongly affect membrane performance. Characterization after filtration and cleaning would also be useful to evaluate whether the MOF particles remain stable within the polyamide layer during operation.

Additional characterization could help explain the relationship between membrane structure and performance. More consistent cross-sectional SEM images, or transmission electron microscopy (TEM), could provide better information about the MOF distribution in the selective layer. Atomic force microscopy (AFM) could be used to study surface roughness, while zeta potential measurements could help evaluate membrane surface charge, which is relevant for PFAS–membrane interactions.

Longer filtration experiments are also needed to better understand membrane durability, fouling, and cleaning behavior. Future tests could include longer operation times, repeated filtration-cleaning cycles, and feed waters containing natural organic matter or inorganic ions to better represent real drinking water conditions. Since PFAS filtration in this work was performed at one TMP, future experiments should also test different TMP values to identify more suitable operating conditions. Temperature effects could also be investigated.

Finally, future studies should consider how to manage the PFAS-rich concentrate produced by nanofiltration. Since membranes separate PFAS rather than destroy them, the concentrate requires further treatment. Combining nanofiltration with adsorption or PFAS destruction technologies could provide a more complete and sustainable treatment process.

Appendices

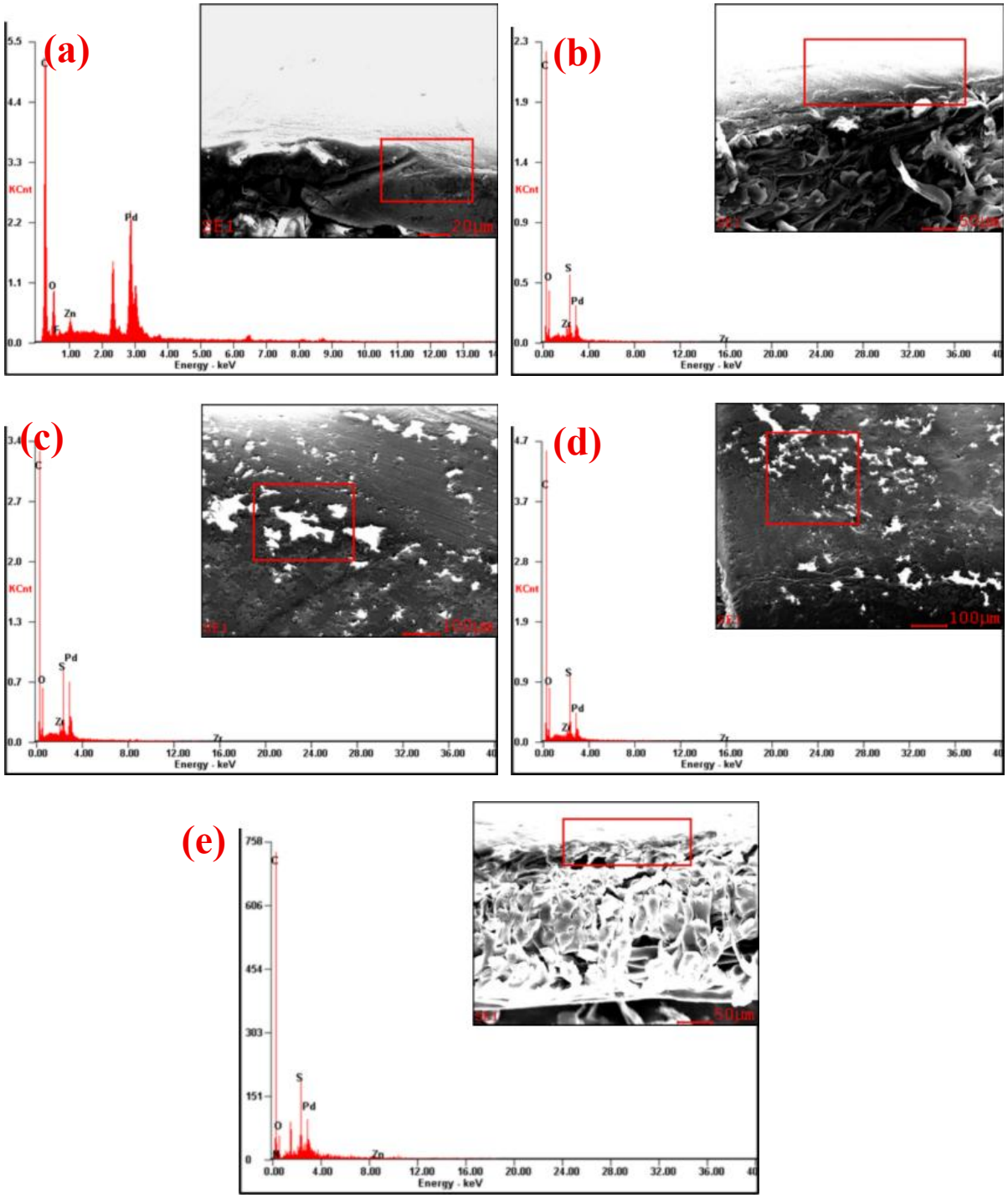

Figure of surface area measured by SEM-EDX and the element detected for: (a)PSf+PA+ZIF-8 0.1 (w/v) %, (b) PSf+PA+ZIF-8 0.2 (w/v) %, (c) PSf+PA+UiO-66-NH_2 0.1 (w/v) %, (d) PSf+PA+UiO-66-NH_2 0.2 (w/v) %, (e) PSf+PA+ZIF-94 0.2 (w/v) %.

Table A. PFAS compounds in FX19 (Adapted from Kakati, 2024 & Wang et al., 2017).

PFAS Compound	Category
PFBA (C4)	Carboxylic acid, short-chain
PFPeA (C5)	Carboxylic acid, short-chain
PFHxA (C6)	Carboxylic acid, short-chain
PFHpA (C7)	Carboxylic acid, short-chain
PFOA (C8)	Carboxylic acid, long-chain
PFNA (C9)	Carboxylic acid, long-chain
PFDA (C10)	Carboxylic acid, long-chain
PFUnDA (C11)	Carboxylic acid, long-chain
PFDoDA (C12)	Carboxylic acid, long-chain
PFTeDA (C14)	Carboxylic acid, long-chain
PFBS (C4)	Sulfonic acid, short-chain
PFHxS (C6)	Sulfonic acid, long-chain
PFOS (C8)	Sulfonic acid, long-chain
FOSA (C8)	Sulfonamide, PFOS-related precursor
6:2 FTSA (C8)	Fluorotelomer sulfonic acid, PFAS precursor

Table B. Detailed data of water permeability, PFAS filtration flux, FF, and FRR.

Membrane	Lp1 (LMH/bar)	Lp2 (LMH/bar)	Lp3 (LMH/bar)	PFAS flux at 10 bar	FF (%)	FRR (%)
PSf support	37.0	14.6	10.9	225.0	60.5	29.6
PSf+PA	2.0	1.7	2.4	19.0	12.7	123.6
UiO-66-NH_2 0.05%	2.3	2.1	2.9	19.4	8.1	126.8
UiO-66-NH_2 0.1%	8.3	6.0	6.6	62.1	28.0	79.0
ZIF-8 0.1%	6.2	5.7	5.5	67.5	8.1	89.5
ZIF-8 0.2%	3.8	3.8	4.5	37.5	0.8	118.3

Table C. Detailed data of preliminary PWF result from Zaragoza.

Membrane	Flux (L/m2.h)			
	0.10%		0.20%	
	7 bar	10 bar	7 bar	10 bar
PSf support	105.5	127.2	105.5	127.2
PSf+PA	6.8	13.5	6.8	13.5
PSf+PA+ZIF-8	9.8	12.7	24.7	40.4
PSf+PA+ZIF-94	12.6	13.6	9.1	12.9
PSf+PA+ZIF-L	0.0	0.0	-	-
PSf+PA+NH2-ZIF-8	0.0	5.0	0	0
UiO-66-NH_2	27.6	32.8	0	0

References

Aghajanzadeh, M., Zamani, M., & Molavi, H. (2018). Preparation of metal–organic frameworks UiO-66 for adsorptive removal of methotrexate from aqueous solution. *Journal of Inorganic and Organometallic Polymers and Materials, 28*, 177–186. https://doi.org/10.1007/s10904-017-0709-3

Alam, A., Ahmad, J., Shah, M. U. H., Asmatullah, Khan, H., & Ali, W. (2026). Recent advances in MOF synthesis and their applications in mixed-matrix membranes for water treatment: A critical review. *Microchemical Journal, 221*, 116982. https://doi.org/10.1016/j.microc.2026.116982

Baker, R. W. (2012). *Membrane technology and applications* (3rd ed.). John Wiley & Sons. https://doi.org/10.1002/9781118359686

Bi, Y., Meng, X., Tan, Z., Geng, Q., Peng, J., Yong, Q., Sun, X., Guo, M., & Wang, X. (2024). A novel ZIF-L/PEI thin film nanocomposite membrane for removing perfluoroalkyl substances (PFASs) from water: Enhanced retention and high flux. *Science of the Total Environment, 925*, 171727. https://doi.org/10.1016/j.scitotenv.2024.171727

Buck, R. C., Franklin, J., Berger, U., Conder, J. M., Cousins, I. T., de Voogt, P., Jensen, A. A., Kannan, K., Mabury, S. A., & van Leeuwen, S. P. J. (2011). Perfluoroalkyl and polyfluoroalkyl substances in the environment: Terminology, classification, and origins. *Integrated Environmental Assessment and Management, 7*(4), 513–541. https://doi.org/10.1002/ieam.258

Casella, G. S., Miranda, M. M., Drumond, G. P., Silva, G. O. R., Zouaoui, F., Arcanjo, G. S., Amaral, M. C. S., de Paula, E. C., & Moreira, V. R. (2026). Recent developments in membrane treatment technologies for PFAS removal from surface and groundwater. *Journal of Environmental Chemical Engineering, 14*, 120598. https://doi.org/10.1016/j.jece.2025.120598

Cavka, J. H., Jakobsen, S., Olsbye, U., Guillou, N., Lamberti, C., Bordiga, S., & Lillerud, K. P. (2008). A new zirconium inorganic building brick forming metal organic frameworks with exceptional stability. *Journal of the American Chemical Society, 130*(42), 13850–13851. https://doi.org/10.1021/ja8057953

Furukawa, H., Cordova, K. E., O'Keeffe, M., & Yaghi, O. M. (2013). The chemistry and applications of metal-organic frameworks. *Science, 341*(6149), 1230444. https://doi.org/10.1126/science.1230444

Gyllenhammar, I., Benskin, J. P., Plassmann, M., Kruså, M., McCleaf, P., Hedvall Kallerman, P., Lampa, E., & Glynn, A. (2025). PFAS in first-time mothers from Sweden: Temporal trends and the impact from fish/seafood consumption and drinking water exposure. *Environment International, 202*, 109671. https://doi.org/10.1016/j.envint.2025.109671

Hammarstrand, S., Jakobsson, K., Andersson, E., Xu, Y., Li, Y., Olovsson, M., & Andersson, E. M. (2021). Perfluoroalkyl substances (PFAS) in drinking water and risk for polycystic ovarian syndrome, uterine leiomyoma, and endometriosis: A Swedish cohort study. *Environment International, 157*, 106819. https://doi.org/10.1016/j.envint.2021.106819

Idarraga-Mora, J. A., Lemelin, M. A., Weinman, S. T., & Husson, S. M. (2019). Effect of short-term contact with C1–C4 monohydric alcohols on the water permeance of MPD–TMC thin-film composite reverse osmosis membranes. *Membranes, 9*(8), 92. https://doi.org/10.3390/membranes9080092

Jo, J. H., Lee, C. O., Ryu, G. Y., Jae, H., Roh, D., & Chi, W. S. (2022). Hierarchical amine-functionalized ZIF-8 mixed-matrix membranes with an engineered interface and transport pathway for efficient gas separation. *ACS Applied Polymer Materials, 4*(9), 6426–6439. https://doi.org/10.1021/acsapm.2c00843

Kakati, S. (2024). Prediction of removal of per- and poly-fluoroalkyl substances (PFAS) from drinking water by nanofiltration and reverse osmosis membranes: Analysing membrane flux variation over time and their ion removal efficiency [Master's thesis, Lund University].

Kim, K. Y., Ekpe, O. D., Lee, H.-J., & Oh, J.-E. (2020). Perfluoroalkyl substances and pharmaceuticals removal in full-scale drinking water treatment plants. *Journal of Hazardous Materials, 400*, 123235. https://doi.org/10.1016/j.jhazmat.2020.123235

Le, T., Jamshidi, E., Beidaghi, M., & Esfahani, M. R. (2022). Functionalized-MXene thin-film nanocomposite hollow fiber membranes for enhanced PFAS removal from water. *ACS Applied Materials & Interfaces, 14*(22), 25397–25408. https://doi.org/10.1021/acsami.2c03796

Liu, C., Ho, H.-J., & Iizuka, A. (2025). Filtration and electrical membrane-based treatment methods for PFAS-contaminated water and preparation methods for the membranes employed. *Applied Water Science, 15*, 290. https://doi.org/10.1007/s13201-025-02644-6

Martínez-Izquierdo, L., Téllez, C., & Coronas, J. (2022). Highly stable Pebax® Renew® thin-film nanocomposite membranes with metal organic framework ZIF-94 and ionic liquid [Bmim][BF_4] for CO_2 capture. *Journal of Materials Chemistry A, 10*(36), 18822–18833. https://doi.org/10.1039/D2TA03958C

Mashkoor, F., Shoeb, M., Mashkoor, R., Kalam, A., & Jeong, C. (2026). Coordination-engineered MOFs for PFAS "forever chemicals" remediation: From molecular recognition to capture-to-destruction architectures. *Coordination Chemistry Reviews, 559*, 217818. https://doi.org/10.1016/j.ccr.2026.217818

Min, H. J., Kim, M.-B., Bae, Y.-S., Thallapally, P. K., Lee, J. H., & Kim, J. H. (2023). Polymer-infiltrated metal–organic frameworks for thin-film composite mixed-matrix membranes with high gas separation properties. *Membranes, 13*(3), 287. https://doi.org/10.3390/membranes13030287

Mulder, M. (1996). *Basic principles of membrane technology* (2nd ed.). Kluwer Academic Publishers. https://doi.org/10.1007/978-94-009-1766-8

Muramba, F. M., Ncube, S., Makhetha, T. A., & Seopela, M. P. (2026). Modification of cellulose acetate-supported thin film composite membrane with amine-functionalized ZIF-8 (NH_2-ZIF-8) nanofillers for potential greywater reclamation. *Desalination and Water Treatment, 326*, 101777. https://doi.org/10.1016/j.dwt.2026.101777

Park, K. S., Ni, Z., Côté, A. P., Choi, J. Y., Huang, R., Uribe-Romo, F. J., Chae, H. K., O'Keeffe, M., & Yaghi, O. M. (2006). Exceptional chemical and thermal stability of zeolitic imidazolate frameworks. *Proceedings of the National Academy of Sciences, 103*(27), 10186–10191. https://doi.org/10.1073/pnas.0602439103

Pervov, A., & Spitsov, D. (2023). Control of the ionic composition of nanofiltration membrane permeate to improve product water quality in drinking water supply applications. *Water, 15*(16), 2970. https://doi.org/10.3390/w15162970

Petersen, R. J. (1993). Composite reverse osmosis and nanofiltration membranes. *Journal of Membrane Science, 83*(1), 81–150. https://doi.org/10.1016/0376-7388(93)80014-O

Pham, M.-X., Le, T. M., Tran, T. T., Ha, H. K. P., Phong, M. T., Nguyen, V.-H., & Tran, L.-H. (2021). Fabrication and characterization of polyamide thin-film composite membrane via interfacial polycondensation for pervaporation separation of salt and arsenic from water. *RSC Advances, 11*(63), 39657–39665. https://doi.org/10.1039/D1RA07492J

Pina-Vidal, C., Berned-Samatán, V., Piera, E., Caballero, M. Á., & Téllez, C. (2024). Mechanochemical encapsulation of caffeine in UiO-66 and UiO-66-NH_2 to obtain polymeric composites by extrusion with recycled polyamide 6 or polylactic acid biopolymer. *Polymers, 16*(5), 637. https://doi.org/10.3390/polym16050637

Pla, R., Alonso-Morales, N., Baeza, J. A., Calvo, L., & Gilarranz, M. A. (2025). Removal of PFAS from complex matrix water by filtration with supported graphene oxide membranes. *Journal of Environmental Chemical Engineering, 13*(6), 120225. https://doi.org/10.1016/j.jece.2025.120225

Refaat, D., Yahia, M., & Coronas, J. (2024). Thin film nanocomposite membranes based on renewable polymer Pebax® and zeolitic imidazolate frameworks for CO_2/CH_4 separation. *Process Safety and Environmental Protection, 192*, 401–411. https://doi.org/10.1016/j.psep.2024.10.053

Thompson, J. A., Brunelli, N. A., Lively, R. P., Johnson, J. R., Jones, C. W., & Nair, S. (2013). Tunable CO_2 adsorbents by mixed-linker synthesis and postsynthetic modification of zeolitic imidazolate frameworks. *The Journal of Physical Chemistry C, 117*(16), 8198–8207. https://doi.org/10.1021/jp312590r

Wang, Z., DeWitt, J. C., Higgins, C. P., & Cousins, I. T. (2017). A never-ending story of per- and polyfluoroalkyl substances (PFASs)? *Environmental Science & Technology, 51*(5), 2508–2518. https://doi.org/10.1021/acs.est.6b04806

Zhang, K., Cheng, P., Liu, Y., & Xia, S. (2024). Efficient removal of per- and polyfluoroalkyl substances by a metal-organic framework membrane with high selectivity and stability. *Water Research, 265*, 122276. https://doi.org/10.1016/j.watres.2024.122276